NASA CONTRACTOR REPORT

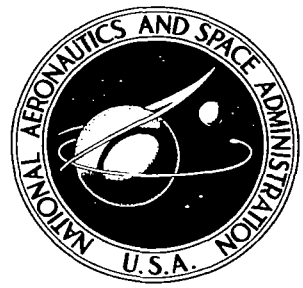

NASA CR-506

ELECTRODE PHENOMENA IN HIGH ENERGY DENSITY DISCHARGES AS APPLIED TO PLASMA ACCELERATION PROBLEMS

by Helmut Poppa

Prepared by
GENERAL DYNAMICS CORPORATION
San Diego, Calif.
for

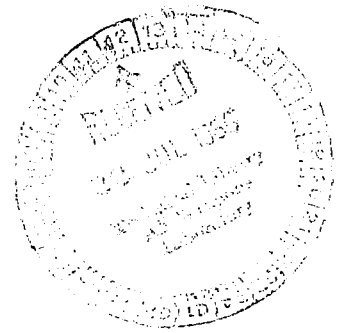

NATIONAL AERONAUTICS AND SPACE ADMINISTRATION • WASHINGTON, D. C. • JULY 1966

ELECTRODE PHENOMENA IN HIGH ENERGY DENSITY DISCHARGES AS APPLIED TO PLASMA ACCELERATION PROBLEMS

By Helmut Poppa

Prepared under Contract No. NASw-1103 by
GENERAL DYNAMICS CORPORATION
San Diego, Calif.

for

NATIONAL AERONAUTICS AND SPACE ADMINISTRATION

For sale by the Clearinghouse for Federal Scientific and Technical Information
Springfield, Virginia 22151 – Price $3.00

ABSTRACT

Plasma-electrode interactions were investigated, studying in detail microscopic and submicroscopic changes in electrode surface structure and morphology.

Transmission electron microscopy of crystallographically well defined thin foil electrodes showed that the orientation dependence of the sputtering yield is weak for low ion energies. Specifically, the difference in sputtering yield for (100) and (111) oriented gold foils (50 eV to 500 eV argon ion energy) is of the order of 15%; use of properly oriented single crystal discharge electrodes, therefore, will not reduce electrode destruction significantly, even if ion bombardment sputtering should be the major cause for electrode disintegration.

Transmission electron diffraction of Cu foils bombarded with 500 eV nitrogen ions (ion beam intensity ~ 0.07 mA/cm^2) revealed no sign of chemical corrosion attack, another possible mechanism of electrode disintegration. Reflexion electron diffraction of a bulk copper cathode exposed to a nitrogen discharge in a coaxial plasma gun confirmed the negative corrosion results.

Cathode morphologies of two plasma gun types (coaxial and pulsed arc gun) were studied by replica electron microscopy, as they developed during gun operation. Microscopic structure features found on electrode surfaces indicate the existence of small (5 to 50μ) areas of localized surface attack (cathode spots). The attack is so strong that localized melting of the cathode surface occurs. The melting hypothesis was verified by detecting changes in cathode surface crystallography caused by localized melting of cathode material. Future discharge electrode research should concentrate on investigating properties and function of cathode spots.

TABLE OF CONTENTS

ILLUSTRATIONS

1.0 INTRODUCTION

Electrode phenomena in high energy density discharges are an important part of plasma acceleration problems: (1) Metal electrodes are essential to every device used for generating a plasma for acceleration purposes and these electrodes disintegrate during operation. The rate of electrode disintegration varies with the type of accelerator but is generally severe enough to justify the search for improvements. (2) Plasma boundary conditions can be influenced by the surface properties of discharge electrodes. Also, reaction products stemming from the disintegration of electrode surfaces can interact with the plasma. The general properties of a plasma generated between electrodes, therefore, may be influenced strongly by electrode processes.

The importance of electrode phenomena for the understanding of various types of gaseous discharges has been realized long ago. About fifty years of intensive experimental research on gaseous discharges have produced a large amount of (not always consistent) information about the behavior of the electrode components of discharges. However, the problems encountered in simple discharge types are already so complex[1,2] that it is difficult to apply the results to complicated accelerators. Furthermore, plasma researchers sometimes focus their attention on plasma properties, as influenced by electrodes that have unknown surface structure. This complicates correlating changes in electrode surface structure with plasma characteristics and renders even more difficult the investigation of electrode plasma interactions.

This report, which is presented in fulfillment of contract NASw-1103, contains a description of experimental work carried out in the area of plasma-electrode interactions. In the first one-man-year effort the investigation of submicroscopic changes in electrode structures was emphasized and electron microscope methods were used successfully. The studies were concentrated in two major areas: (a) Fundamentally oriented low energy and low beam intensity ion bombardment experiments, conducted inside an electron microscope for immediate and more reliable evaluation of irradiation effects, (b) replica electron microscopy and reflexion electron diffraction studies of the structure of actual plasma gun electrode surfaces.

The ion bombardment work was planned specifically to investigate possibilities of minimizing electrode destruction due to sputtering by discharge ions. At the same time microstructural damage caused by ion irradiation of metal electrodes was to be studied. The experimental approach for these studies was dominated by transmission electron microscopy requirements. Therefore, thin foil electrodes of well defined crystallographic structures had to be used in this part of the work instead of bulk electrodes.

Checking on possible chemical corrosion reactions, arrangements for diffraction studies on bulk copper discharge electrodes were made. Replica studies of electrodes of two different types of plasma guns attempted correlating electrode surface morphology and specific plasma characteristics.

2.0 LOW CURRENT DENSITY ION BOMBARDMENT STUDIES

2.01 Apparatus and experimental method

Work on noble gas ion radiation damage in thin foil specimens has been

conducted in the past.[3,4] The target specimens were prepared in thin film form amenable to transmission electron microscopy analysis before the irradiation, which took place in a vacuum system separate from the electron microscope. Therefore, the irradiated specimens had to be exposed to the laboratory atmosphere during transfer to the electron microscope specimen chamber where they had to be taken for the analysis.

Inspecting an irradiated specimen immediately after ion bombardment is desirable. For this to be possible the irradiations have to be carried out in the electron microscope vacuum system. In this way uncontrollable changes in the specimen microstructure due to transfer problems were avoided and repeated bombardment of the same microscopic target area became feasible. However, for repeated bombardment, one has to solve the problem of carbon specimen contamination by the analyzing electron beam. This can be accomplished through the reduction of residual gas pressures at the site of the specimen (see Poppa[5]). Then the choice had to be made whether to irradiate the target specimen in between microscopy inspections (by moving it to a different bombardment position within the microscope vacuum system) or whether to bombard the specimen in a true in-situ fashion, while observing structural specimen changes at the same time by high resolution transmission microscopy. The latter technique is, of course, the most desirable but also the most complex one experimentally.

There are special design and construction problems, connected with the development of an ion gun and an electron microscope specimen stage that permit true in-situ observation of ion radiation damage in thin single crystals. They prompted us to concentrate all construction efforts

in the first year on the development of the semi in-situ ion bombardment system. Although this enables the investigator studying the target structure only after repeated irradiations it was felt that enough valuable information concerning the physical nature of the disintegration process could be collected in this way. For this reason the development of the more sophicaticated 'true in-situ system' was postponed.

Different types of ion gun designs were examined on a separate vacuum test stand. The design finally selected fulfilled best the special requirements imposed upon the ion generating system by the need for adapting it to the high temperature specimen stage of the HU-11 electron microscope. The ion gun had to be compact, easy to dismantle, and constructed so that a low energy (50 eV to 500 eV) ion beam of small cross section was generated that could be focused on the electron microscope specimen located inside the oven of the heating stage.

In the final design an ion beam is extracted from a higher pressure discharge chamber by a high potential (2.5 keV) Pierce optical system and then decelerated by a series of electrical immersion lenses of cylindrical symmetry. A schematic of the ion gun is given in Figure 1 and a typical set of operating parameters is:

$$U_A = 25 \text{ V (for argon)}$$

$$I_A = 50 \text{ mA}$$

$$U_E = 2.5 \text{ kV}$$

$$U_B = 300 \text{ V}$$

$$I_g = 15 \mu$$

$$I_{sp} = 7 \mu\text{A}$$

$$i_{sp} = 67 \frac{\mu\text{A}}{\text{cm}^2}$$

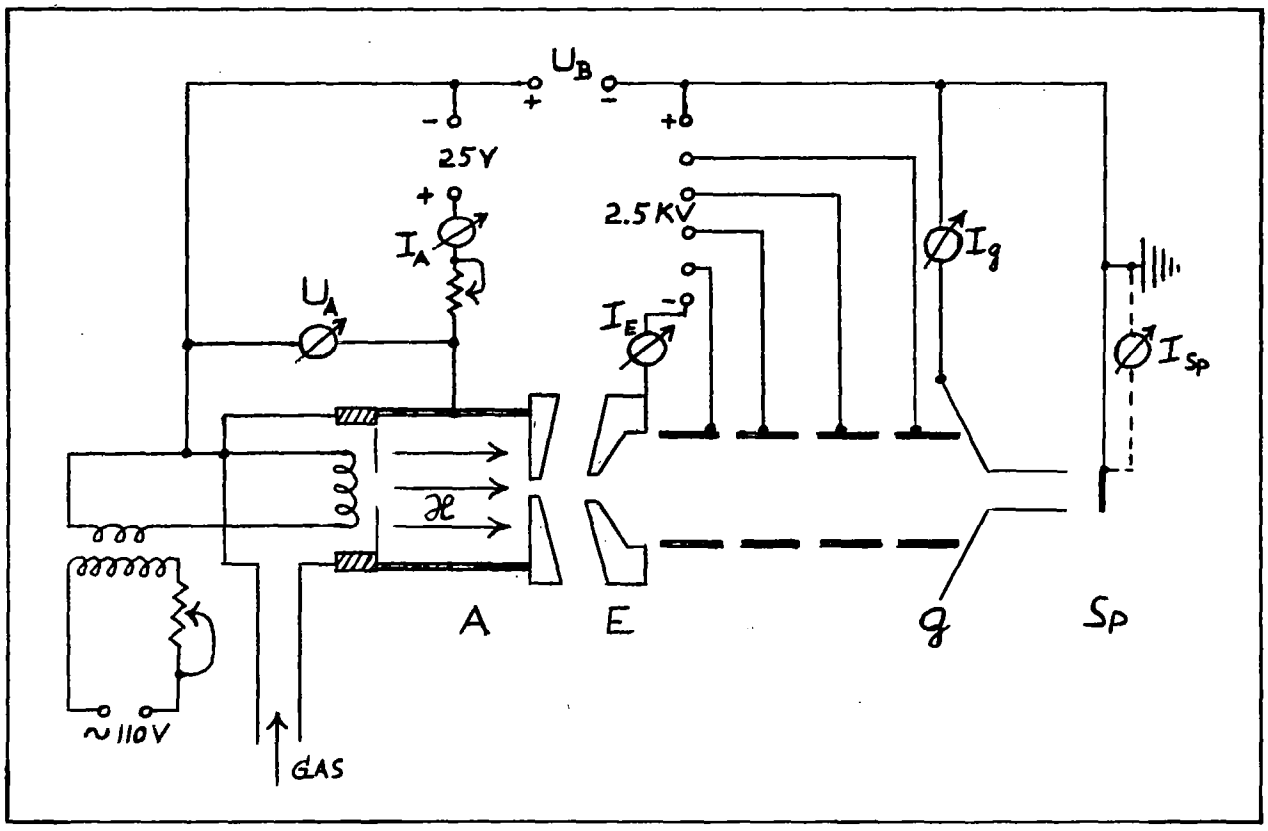

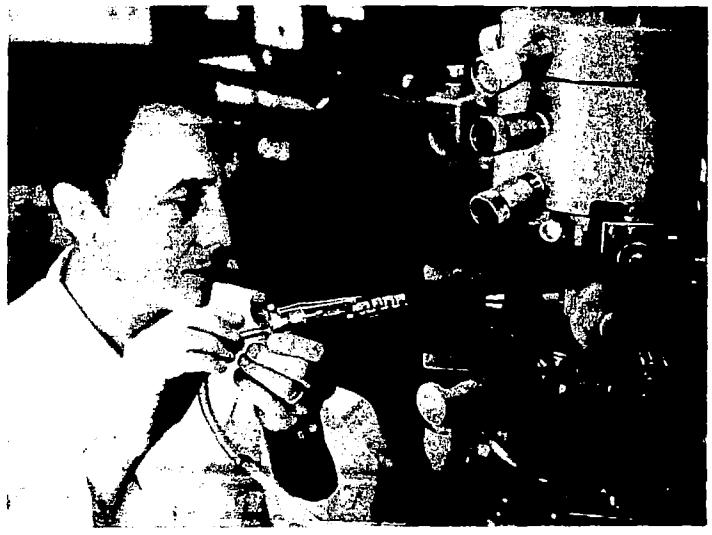

Fig. 1

The performance of the gun was satisfying and also constant over an ion energy range from 100 eV to 500 eV. From 100 eV down to 50 eV, however, the performance fell off rapidly. The ion current density at 50 eV was only about 1/5 of the beam intensity at 100 eV.

The energy spread of the ion beam was estimated with the help of a crude reversed field method (applied between Sp and g, compare the schematic) and found to be of the order of 2% in the energy range used here. High energy neutral gas atoms that could be formed by charge exchange in the acceleration-deceleration part of the gun are neglected throughout our experiments considering the results obtained in a similar system.[4]

After testing in the separate vacuum system, the ion gun was mounted to the specimen exchange window of the electron microscope. Further testing was necessitated by the fact that the actual geometrical arrangement of the last gun electrode g and the target Sp in the microscope specimen stage could not be duplicated outside the microscope with sufficient accuracy. Accurate correlation of the ion currents I_{sp} and I_g is necessary. However, the target being grounded necessarily in the microscope, I_{sp} can only be determined by measuring I_g. Temporarily an additional small probe was inserted into the microscope heating stage for this purpose and the focusing potentials were maximized for ion energies from 50 eV to 500 eV. The ion current densities corresponding to the conditions of best focus were calibrated as a function of I_g. This simple method of determining I_{sp} was retained throughout our experiments, although it is feasible to design a special specimen holder that would permit direct measurement of I_{sp} (and ground the specimen during later microscopy).

Here is room for possible future improvements, more accurate quantitative sputtering yield measurements becoming desirable.

The apparatus was found to function satisfactorily with the exception of an appreciable variation of the ion beam density over small areas of the ~ 2 mm x 2 mm target surface. However, this fact is a disadvantage only as far as exact quantitative sputtering yield measurements are concerned and these are not the goal of our studies. Local variations in ion beam intensities actually are an asset for most qualitative and some of the quantitative bombardment damage tests: It is now possible to study within one specimen the effects of different bombardment doses.

Results, on the conditions for repeated ion bombardment, were also obtained during the initial testing period of the apparatus. It was found that the target specimen had to be heated to over $400^{\circ}C$ during electron microscope inspection if it was desired to subject the same specimen to repeated ion bombardment. For temperatures below ~ $400^{\circ}C$ the very minute carbon-contamination layers that built up on the specimen surface during exposure to the electron beam in the 10^{-5} torr microscope vacuum effected almost total passivation to ion bombardment sputtering. (In this context, one is tempted to suggest applying carbon passivation to discharge electrodes by forming thin evaporated carbon layers on electrode surfaces. But it is known that decomposition of residual hydrocarbons takes place automatically in any discharge with partial hydrocarbon background pressures higher than ~ 10^{-6} torr; it is also possible that the sputtering process of discharge electrodes is essential for retaining certain vital discharge characteristics.)

2.1 Low Energy Argon Ion Bombardment of Single Crystal and Polycrystal Gold Target Foils

2.1.1 Target specimen preparation: Polycrystalline or single crystalline films of a great variety of metals can be prepared by evaporation or sputtering methods. But the target films needed for our ion bombardment experiments had to be extremely uniform in thickness and possess a very smooth surface structure. Preliminary bombardment experiments had given evidence that grain and twin boundaries are obviously the "weak spots" in the target foil. It is along these boundaries where the disintegration process usually initiates. This discovery would, of course, be important if the results were unambiguous. Unfortunately, there is the possibility of explaining the weak spots in a different way: They could also be "thin spots" stemming from the preparation process of the target foil. Forming the target film by evaporation, weak spots are usually created by the merger of individual large grains during the 3-dimensional growth process. The thin spots would also be accompanied by corresponding areas of higher surface roughness.

The target film structure requirements impose quite severe restrictions upon available film preparation techniques, eliminating most of the commonly used methods. Most single crystal or coarse polycrystalline metal films, for instance, are grown on low free surface energy substrate materials at elevated temperatures. This results in a 3-dimensional growth behavior. Accordingly, these metal films become continuous only shortly before they become opaque to electrons (for electron microscope accelerating voltages of 100 kV the thickness limit for transmission microscopy ranges from ~ 700 Å to ~ 2000 Å, depending upon the atomic weight of the metal).

The resulting films are not smooth and they are not uniform in thickness.

The difficulty can be overcome by growing metal films on metallic substrates of higher free surface energy. Thus, gold target films amenable to transmission electron microscopy studies were prepared, adopting epitaxial vacuum deposition techniques. The (111) oriented single crystals were grown on epitaxial silver layers on mica, the (100) oriented crystals on epitaxial silver on NaCl. Coarse polycrystalline gold layers (needed for evaluating the orientation dependence of sputtering yields under an ion beam that varies strongly in density within the target area)were also grown epitaxially. In this case electrolytically polished bulk silver surfaces served as substrates. The respective substrate temperatures and deposition rates are given in Table 1.

The new growth conditions were found resulting in target films that became coherent during very early stages of overgrowth and, therefore, turned out to be uniform in thickness. Figure 2a and 2b represent respective examples of polycrystalline gold films: Figure 2a was grown on quartz at elevated substrate temperatures and shows many small grains still separated by occasional holes in the film. Figure 2b was grown according to Table 1; it shows larger grains and is uniform in thickness.

The high degree of single crystallinity of the target films is demonstrated by Figure 3, an electron diffraction pattern of a (111) oriented gold target.

Fig. 2a

Fig. 2b

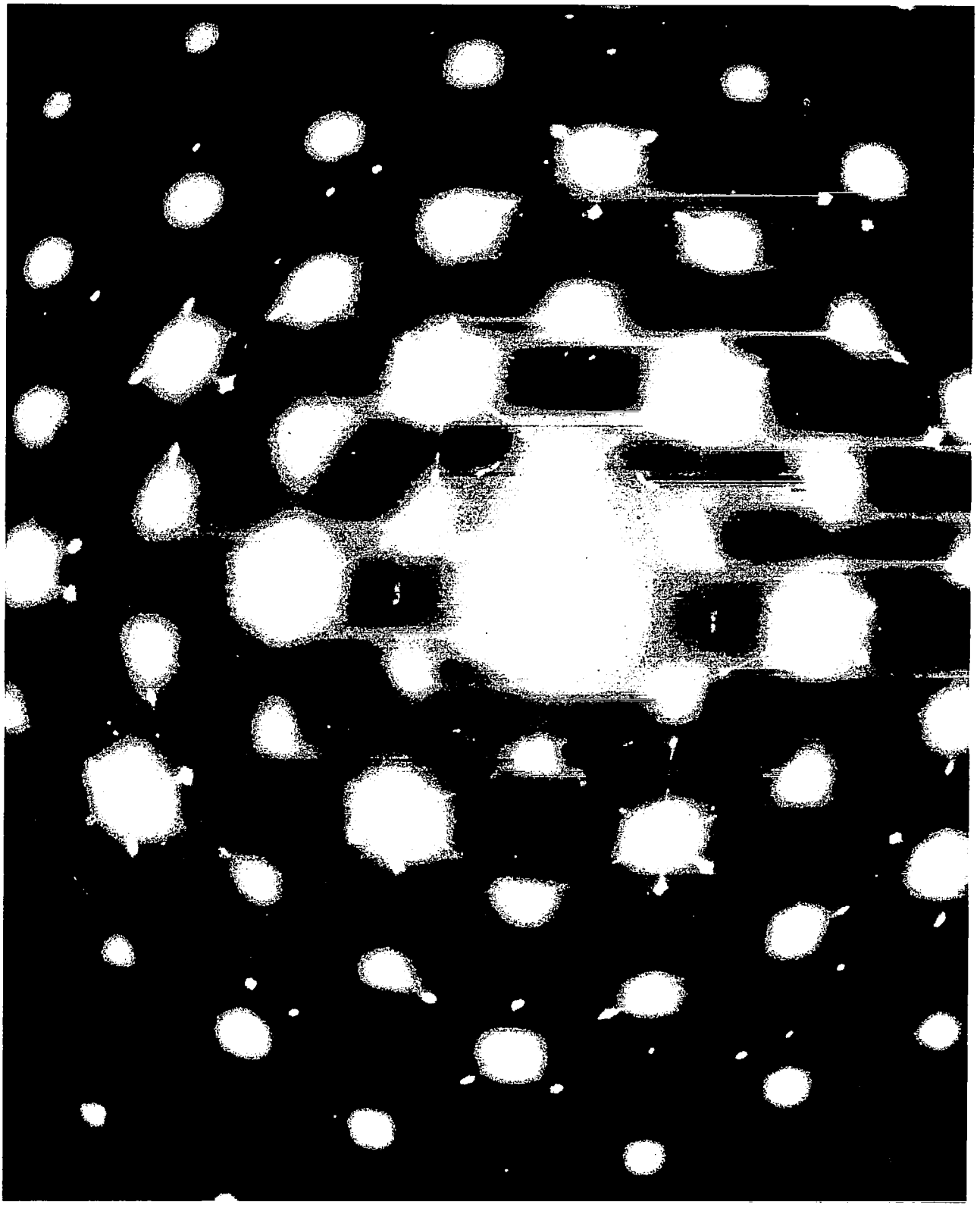

Fig. 3

Orientation of Au Targets	Substrate for Epitaxial Growth	Intermediate Layer of Ag		Final Layer of Au	
		Substr. Temp.	Depos. Rate	Substr. Temp.	Depos. Rate
(111)	mica	280°C	600 Å/min	350°C	1200 Å/min
(100)	NaCl	250°C	700 Å/min	250°C	700 Å/min
Polycryst	Bulk Ag (el. pol.)	250°C	700 Å/min	250°C	700 Å/min

TABLE 1

2.1.2 Radiation damage and etching: Gold target films of 600 Å to 700 Å thickness were subjected to bombardment with Ar^+ ions of energies from 100 eV to 500 eV. However, the observed radiation damage effects were essentially independent of ion energy in the said range, and it was not the purpose of this work to measure sputtering yields quantitatively. Therefore, most of the work reported was carried out at 500 eV. The irradiation times ranged from 5 min to 20 min, mostly around 10 min, but the time of bombardment is not an important parameter in these studies, considering the appreciable differences in ion beam densities within the target area.

The Figure's 4a, 4b, and 4c show radiation damage effects in (111), (100), and polycrystalline Au targets as revealed by transmission electron microscopy. For reasons of comparison Figure 4d is added in which most of the damage, which can be seen as dark dots and short dark dislocation lines, was removed by subsequent annealing treatment.

The nature of this type of radiation damage was studied in detail by others[6] and defined as interstitial point defect clusters and subsurface dislocations. The damage is localized at the surface of the target to a

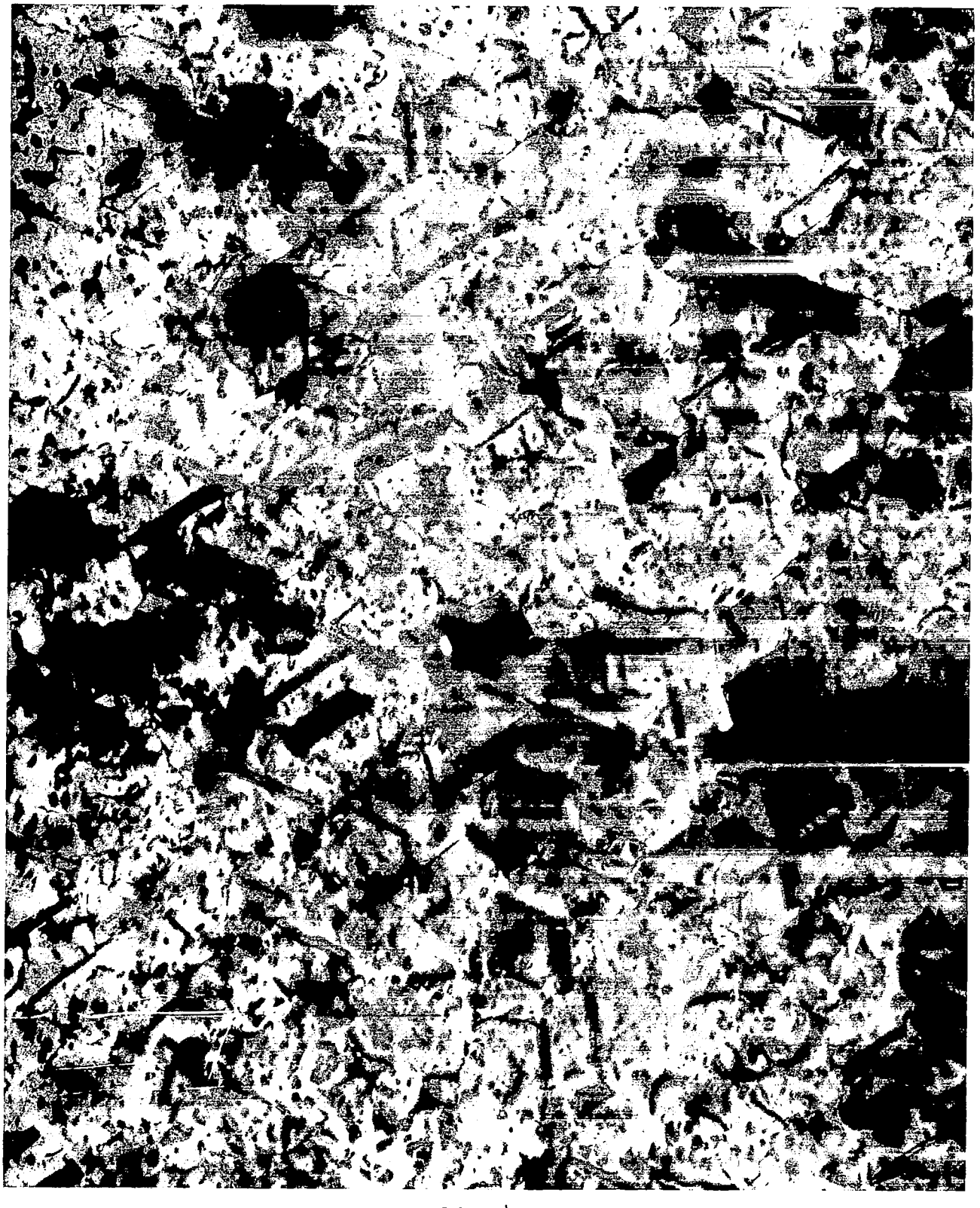

Fig. 4a

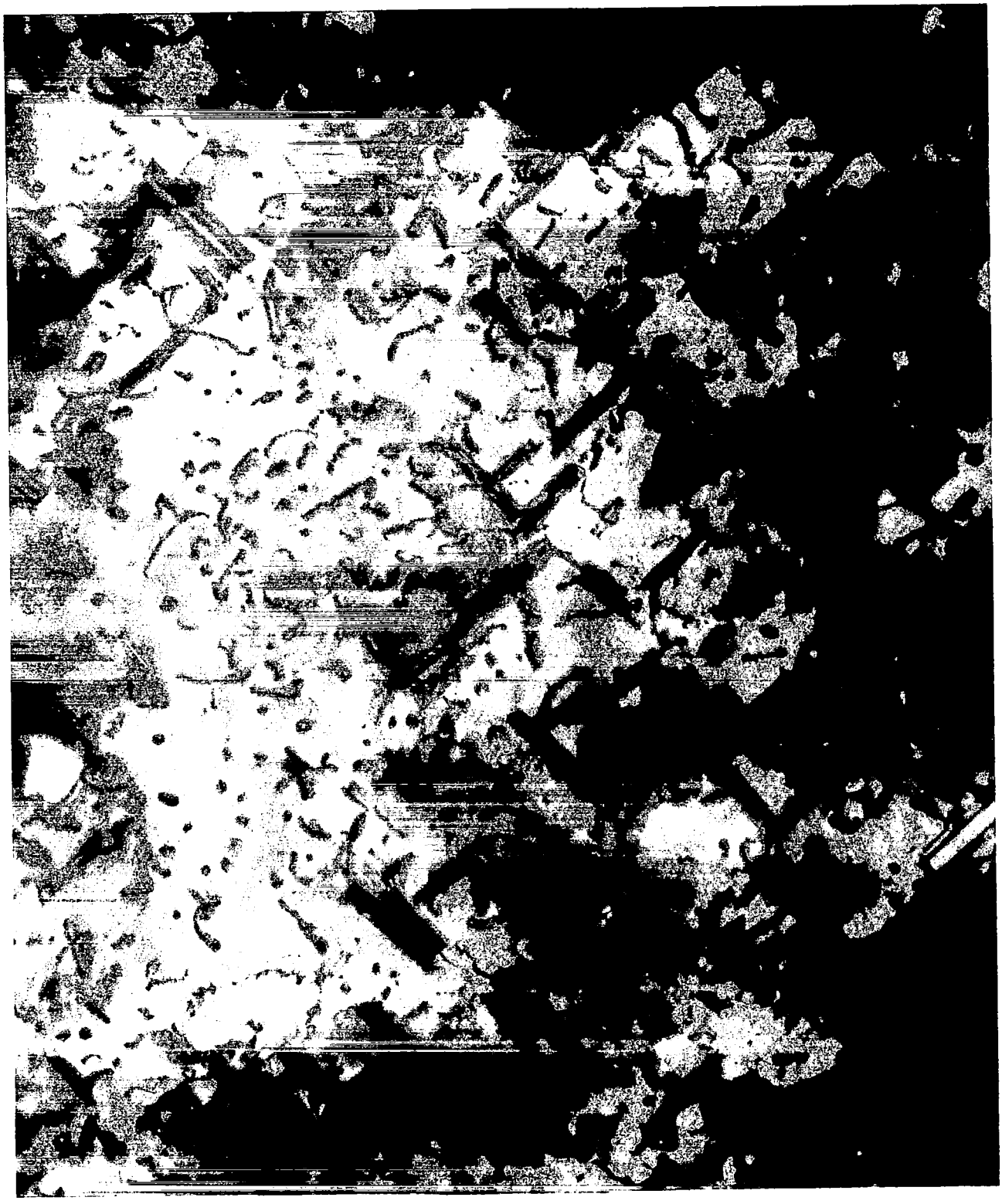

Fig. 4b

Fig. 4c

Fig. 4d

depth of about 100 Å (for 500 eV Ar^+ ions) and formed by direct impingement of replacement sequences aided by local thermal activation from displacement spikes in the gold lattice. It is plausible assuming that a slow single interstitial is created during bombardment with an energy of migration not less than 0.7 eV.

In target areas where the impinging Ar^+ ion flux was higher the structure of the Au targets is quite different (Figure 5). Resulting from the high irradiation dose in these areas, holes are etched into the target. The three-fold (for (111) orientation) or four-fold (for (100) orientation) symmetry of these holes is directly related to the crystallographic structure of the target film. It can also be noted that the predominant lattice defects visible in these micrographs, namely microtwins, stacking faults, and coherent twin boundaries extend along directions which are parallel to the edges of the holes. This behavior shall be explained later in terms of preferred nucleation of argon interstitials at lattice defects.

2.1.3 Heat treatment of target foils after bombardment: The use of an ion gun connected to an electron microscope specimen heating stage permits heat treatment of the target specimens immediately after bombardment. At the same time respective changes in the specimen microstructure can be observed. With the help of this technique tiny round and bright spots were found appearing in the target structure; they grew in size during annealing times of 30 min and longer. Similar features had been observed before[3] and were identified as microscopic argon gas bubbles formed by the clustering of injected argon interstitials which become mobile at elevated target temperatures (350°C annealing temperature).

Fig. 5a

Fig. 5b

Fig. 5c

The important new feature of these argon clusters is their preferred precipitation at coherent twin boundaries, microtwins, grain boundaries, and dislocations. This is demonstrated by Figure 6a ((111) orientation), Figure 6b (polycryst. film) and Figure 6c which is a higher magnification of 6a. A similar behavior is observed in (100) films.

This result can be explained in terms of heterogeneous nucleation theory concepts: A further free energy term is added to the thermodynamic driving force for homogeneous nucleation, stemming from strain energy release at lattice distortions.[7] Consequently, lattice defects and grain boundaries become locations of preferred nucleation and the diffusion of argon interstitials being controlled most probably by the diffusion of lattice vacancies, the preferred nucleation of argon interstitials is also an indication of the nucleation behavior of vacancies. Our results are in good agreement with related work on the precipitation of vacancies at grain boundaries.[8]

2.1.4 Sputtering yield considerations: In applying this mechanism of preferred nucleation of injected gas interstitials at lattice defect sites to the problem of disintegration of metal targets by sputtering attack, one cannot escape the conclusion that these lattice defect sites should also be locations of preferred sputtering attack. This is demonstrated in a striking way by the formation of holes of well defined shape in single crystal films (see Figures 5a and 5b) and by preferred grain boundary attack in polycrystal gold, Figure 5c). Buth whether this effect is large enough to influence the microscopic sputtering yield of bulk metal targets (eventually by such secondary effects as increased

Fig. 6a

Fig. 6b

Fig. 6c

angle of ion incidence at preferably etched locations) cannot be assessed with the present experimental technique. It is conceivable that the appreciable differences in the sputtering yield of polycrystals at low ion energies might be explained in this way (see Figure 7). For high ion energies the differences in sputtering yield as a function of crystallographic orientation are so predominant[9,10] (see Figure 8) that a significant influence of the microstructure is very unlikely.

In order to demonstrate these considerations graphically a recently published compilation of sputtering yield data is given in Figure 7 and Figure 8.[11] Although the data of Figure 7 and Figure 8 apply to copper the general trend of the sputtering yields should also hold for gold as another f.c.c. crystal. The graphs show very clearly the wide spread in sputtering yields for polycrystalline targets at low and high energies and the appreciable differences in single crystal yields as a function of orientation, starting with ion energies of 500 eV and higher.

Approaching the problem with a completely different method of investigation, we have verified the fact that in the energy range from 100 eV to 500 eV the sputtering yield differences for gold as a function of crystallographic orientation are very small:

(a) Separate single crystal gold films of (111) and (100) orientation were bombarded with 500 eV argon ions for the same length of time and their thicknesses before and after bombardment were measured by transmission electron microscopy techniques; (the width of microtwins, visible as dark bands in the micrographs, are a direct measure of the film thickness, if the crystallographic orientation of the film is known). Since the

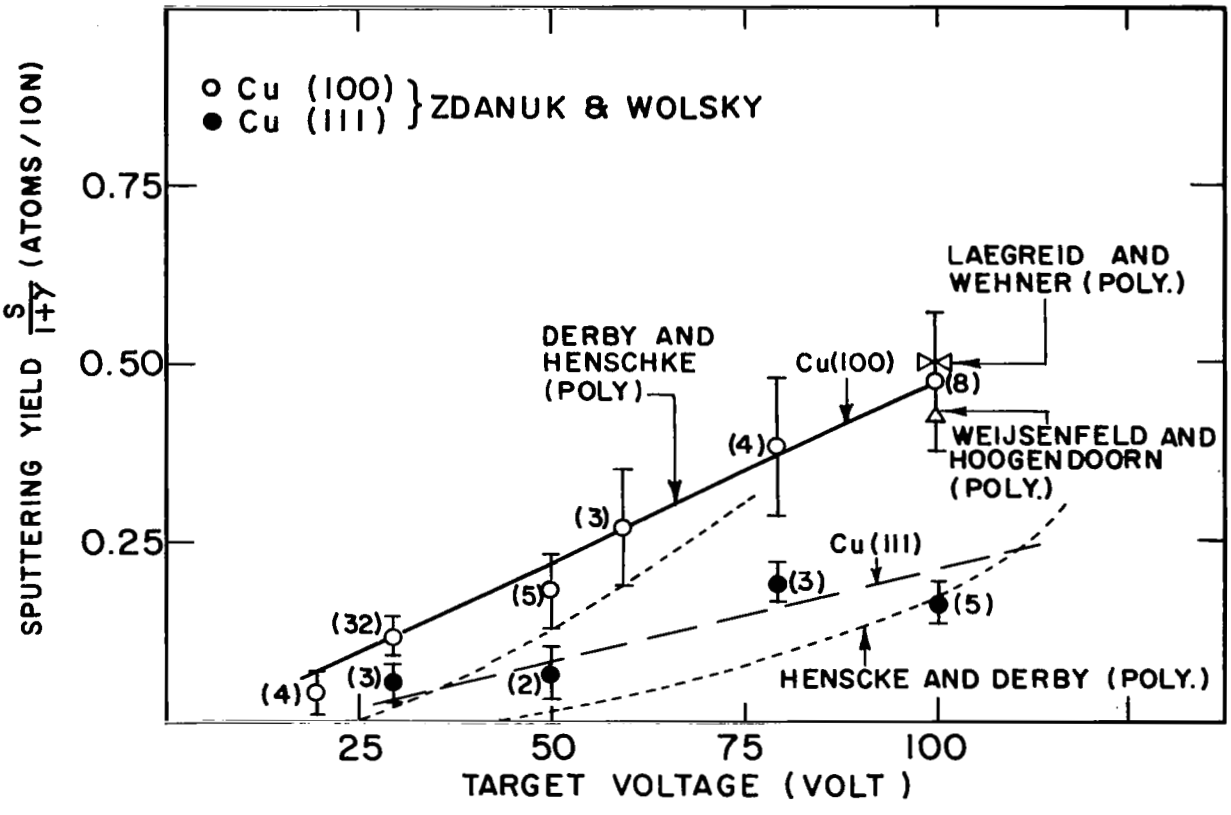
SPUTTERING YIELD $\frac{S}{1+\gamma}$ (ATOMS / ION)
0.75
0.50
0.25
o Cu (100) } ZDANUK & WOLSKY
● Cu (111) }
LAEGREID AND WEHNER (POLY.)
DERBY AND HENSCHKE (POLY)
Cu(100)
(8)
(4)
WEIJSENFELD AND HOOGENDOORN (POLY.)
(3)
Cu(111)
(5)
(3)
(32)
(5)
(4)
(3)
(2)
HENSCKE AND DERBY (POLY.)
25
50
75
100
TARGET VOLTAGE (VOLT)

Fig. 7

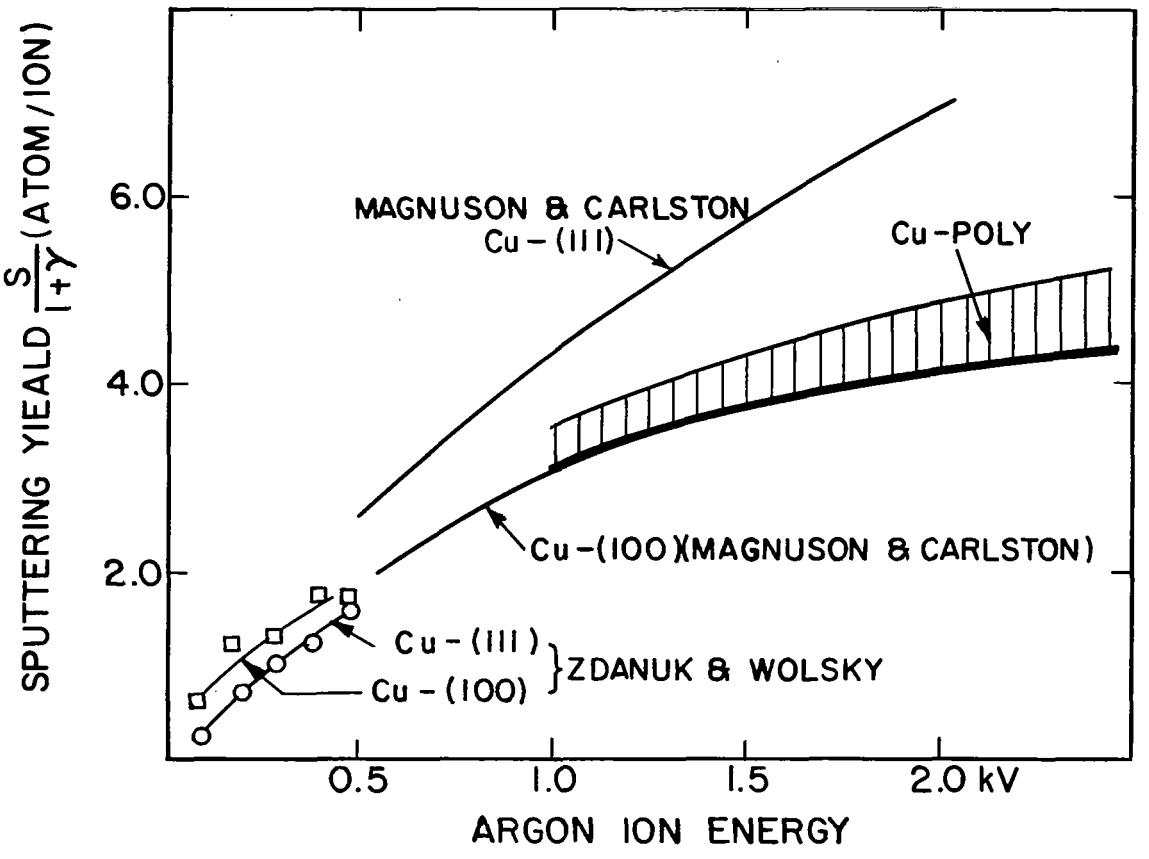
SPUTTERING YIEALD $\frac{S}{1+\gamma}$ (ATOM/ION)
6.0
4.0
2.0
MAGNUSON & CARLSTON
Cu – (111)
Cu-POLY
Cu-(100)(MAGNUSON & CARLSTON)
Cu – (111)
Cu – (100)
}ZDANUK & WOLSKY
0.5
1.0
1.5
2.0 kV
ARGON ION ENERGY

Fig. 8

ion current densities in small target areas could not be measured with sufficient accuracy it was impossible to determine absolute sputtering yields in this way, but relative values were determined:

$$\frac{\text{Sputtering yield (100) - gold}}{\text{Sputtering yield (111) - gold}} = 80\%$$

(b) The uncertainty introduced by ion current density variations over small target areas can be eliminated if thickness variations due to sputtering are measured in adjacent microscopically small gold grains of (100) and (111) orientation. Such grains were found in our polycrystalline gold films and the result for 500 eV ion energy was again:

$$\frac{\text{Sputtering yield (100) - gold}}{\text{Sputtering yield (111) - gold}} = 90\%$$

(c) The small differences in sputtering yields at low ion energies for (100) and (111) gold grains account for another of our bombardment results: No sign of appreciable preferred etching of whole grains of a certain crystallographic orientation was found in any of our polycrystalline targets bombarded almost to destruction with ion energies from 100 eV to 500 eV. This included orientations other than (100) and (111).

One, therefore, has to conclude from our low energy ion bombardment studies (although small quantitative differences are probable for other f.c.c. metal target materials): A mechanism of preferred nucleation of argon interstitials at lattice imperfections is operating which is held responsible for the disintegration of target structures in preferred areas

(grain boundaries in particular). It is conceivable that the same mechanism contributes to the known small differences in sputtering yields of materials of varying degrees of crystallographic perfection for ion energies below 500 eV. This effect is not important in conjunction with the destruction of metal surfaces by higher energy ion sputtering; the influence of crystallographic orientation is much larger.

2.2 Low Energy Nitrogen Ion Bombardment of Highly Oriented Copper Target Foils

2.2.1 Ion gun characteristics and target preparation: The general operating conditions of the ion gun described in paragraph 2.02 remain approximately the same, when switching from argon to nitrogen as discharge gas. However, the maximum ion current output I_{sp} is quite sensitive to small variations in the focusing potentials so that the calibration procedures for I_{sp} as a function of I_g had to be repeated. For this purpose a special probe for the direct measurement of I_{sp} was introduced into the electron microscope specimen stage as described previously. But with nitrogen it was possible to raise the discharge voltage U_A somewhat, the second ionization potential for nitrogen being 29.6 eV instead of 27.6 eV for argon. This resulted in improved I_{sp} values: up to 100% higher, for ion energies from 300 eV to 500 eV. In the ion energy range from 50 eV to 100 eV the ion currents I_{sp} were practically identical for both discharge gases.

In simulating bulk discharge electrode corrosion experiments that will be described later in this report, the target foil material had to be copper. The target foils also had to be crystallographically well defined; they were, therefore, prepared as single crystal (100) oriented films by evaporation (evaporation rate $\sim$ 800 Å/min) onto heated (350°C)

NaCl single crystal substrates. The resulting films are known to be single crystal but can be converted into highly textured Cu_2O films[12] by atmospheric storage. Figure 9a shows a transmission electron diffraction pattern of such a film which was to be used as target film for nitrogen ion bombardment. In this way the always oxidized actual bulk copper electrodes were duplicated in the thin film corrosion tests.

2.2.2 Search for chemical corrosion reaction: The nitrogen ion bombardment experiments of the Cu_2O target films were performed as follows: (1) examination of relatively thick but still electron transparent target films by electron microscopy and diffraction, determining the target microstructure before N^+ bombardment. Transmission micrographs like Figure 9b served mainly as target thickness indicators while the chemical (and crystallographic) composition of the target was analyzed by transmission electron diffraction. (2) N^+ irradiation (ion energy 300 eV), adjusting the bombardment dose so that electron microscopy of the target immediately after the end of bombardment (while retaining the target in the microscope vacuum) showed definite signs of disintegration. The thinning of the target foil can easily be recognized in Figure 10a. Immediately after bombardment another electron diffraction pattern was recorded (Figure 10b).

If any chemical reaction with nonvolatile reaction products had occurred on the target surface as a result of the strong N^+ bombardment, additional Debey-Scherrer diffraction rings would have to show up in Figure 10b, as compared to Figure 9a. However, this is not the case! It is, therefore, impossible to attribute the erosion of cathode surfaces in a nitrogen discharge at least partially to a bombardment induced

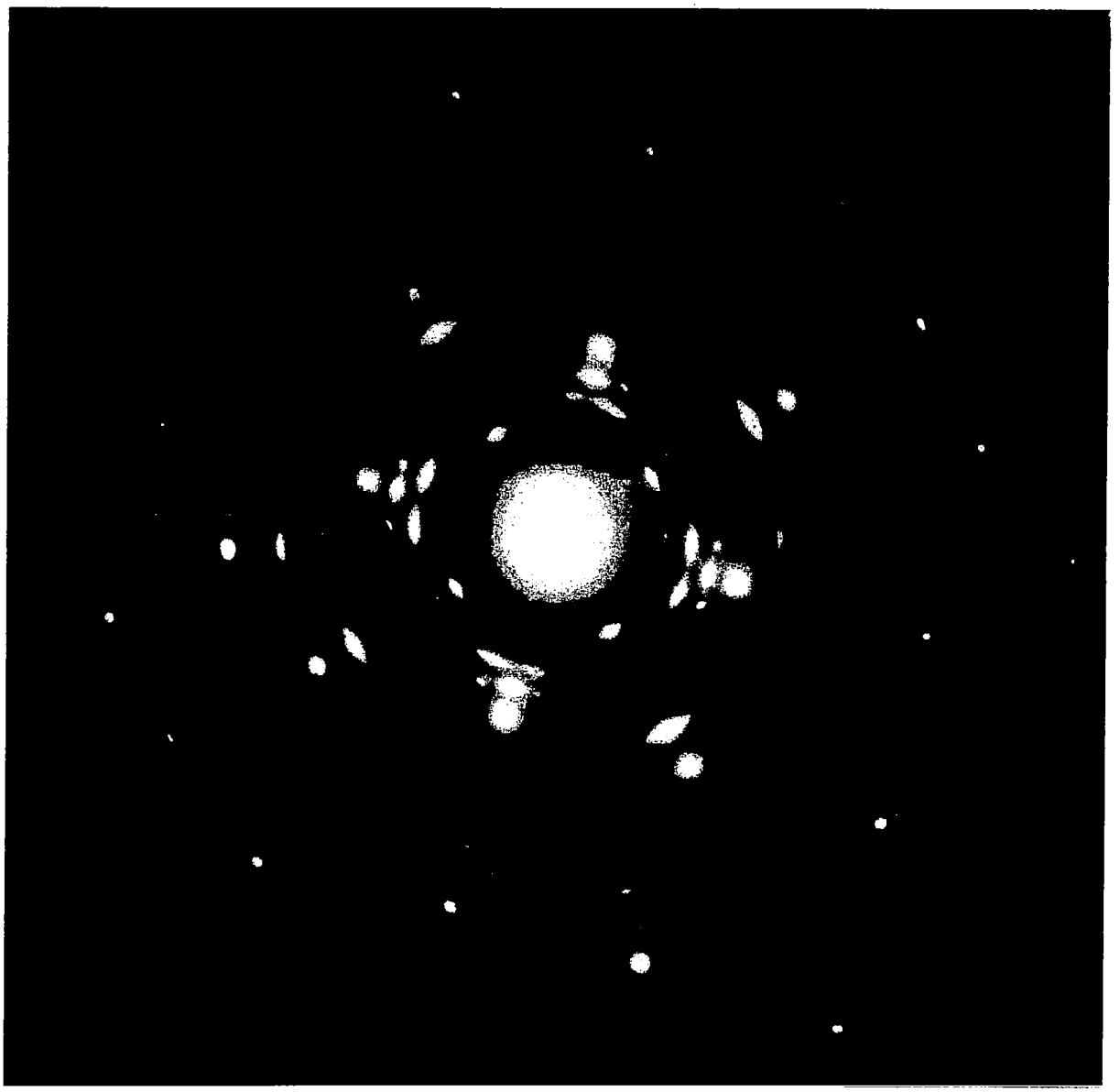

Fig. 9a

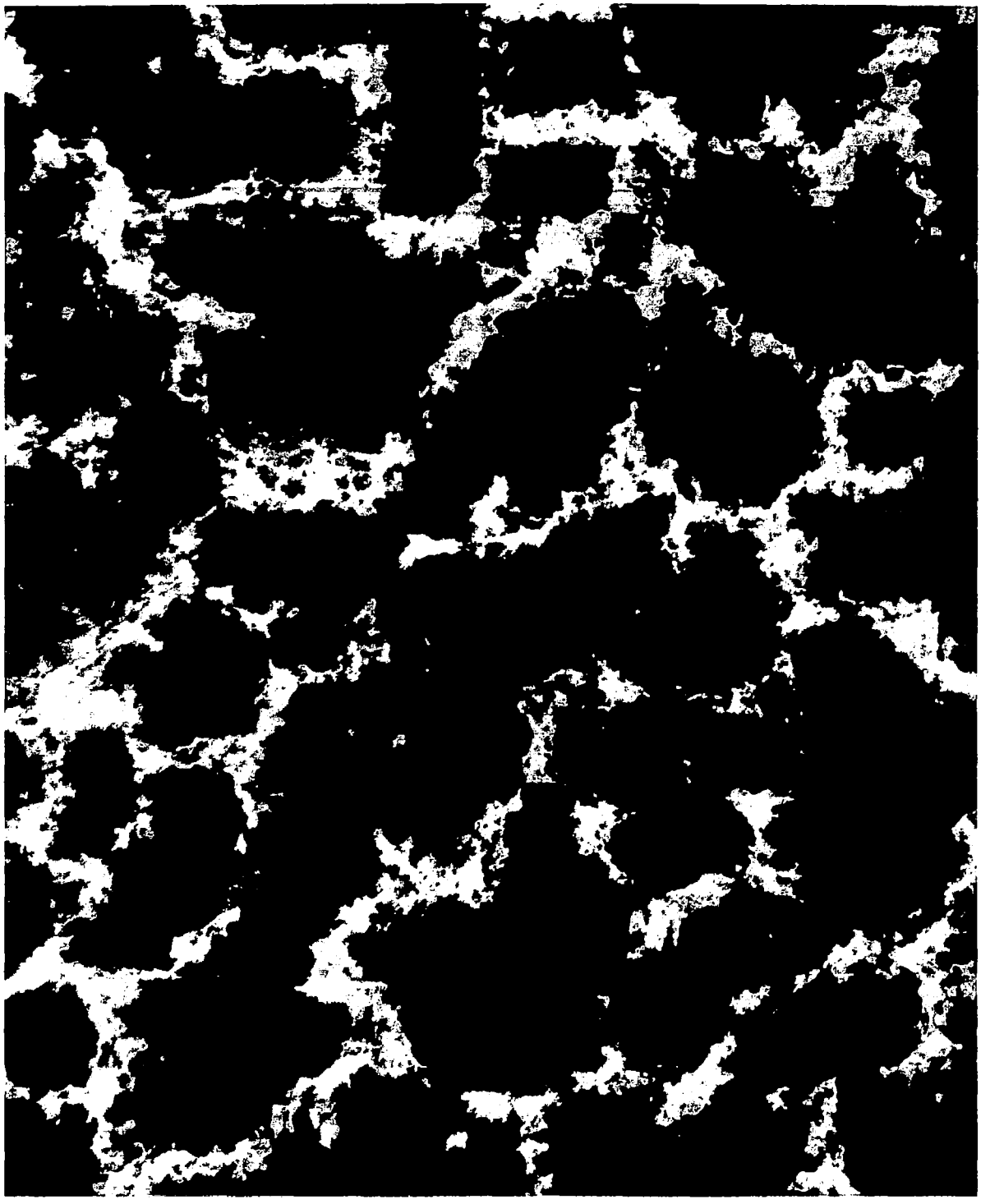

Fig. 9b

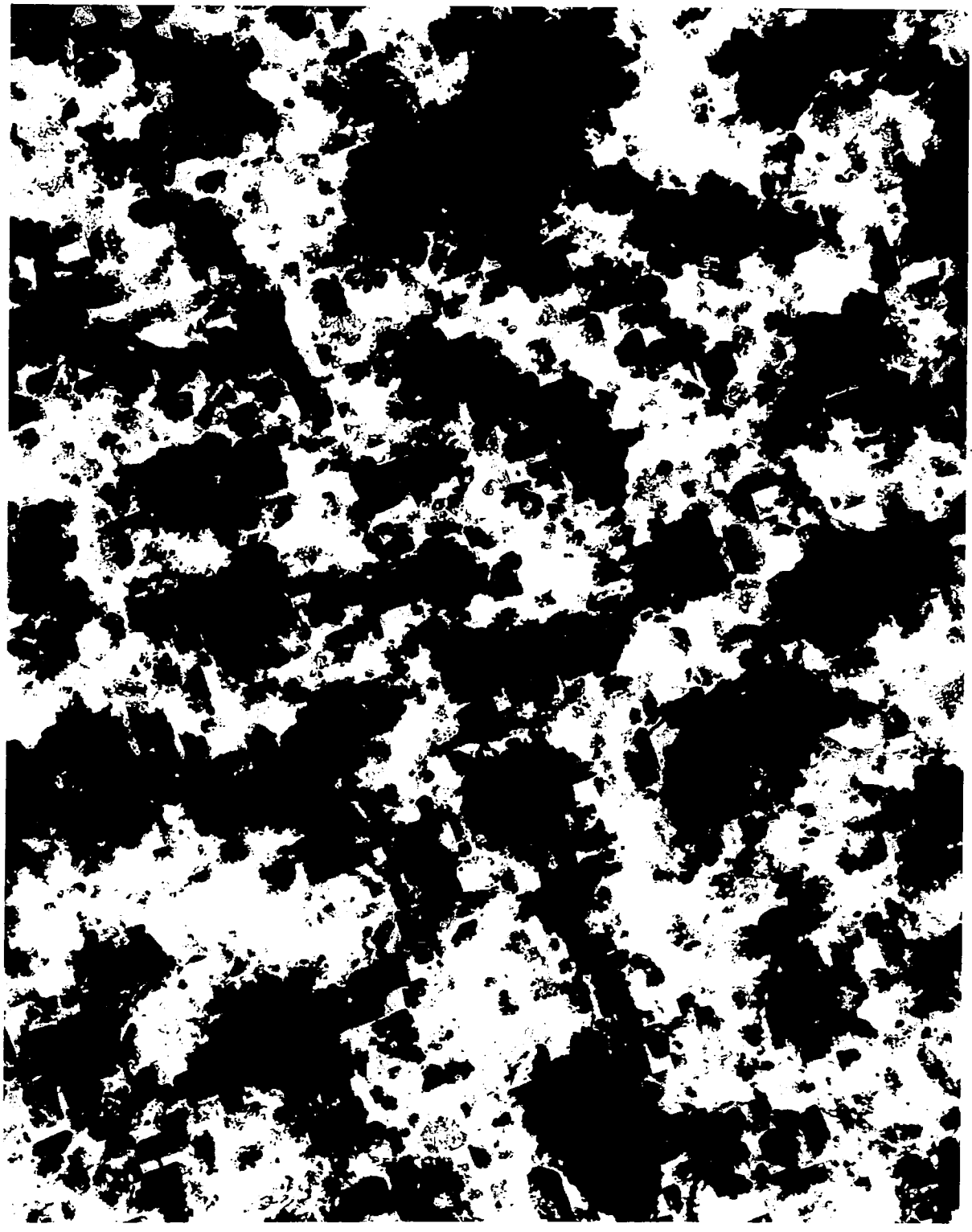

Fig. 10a

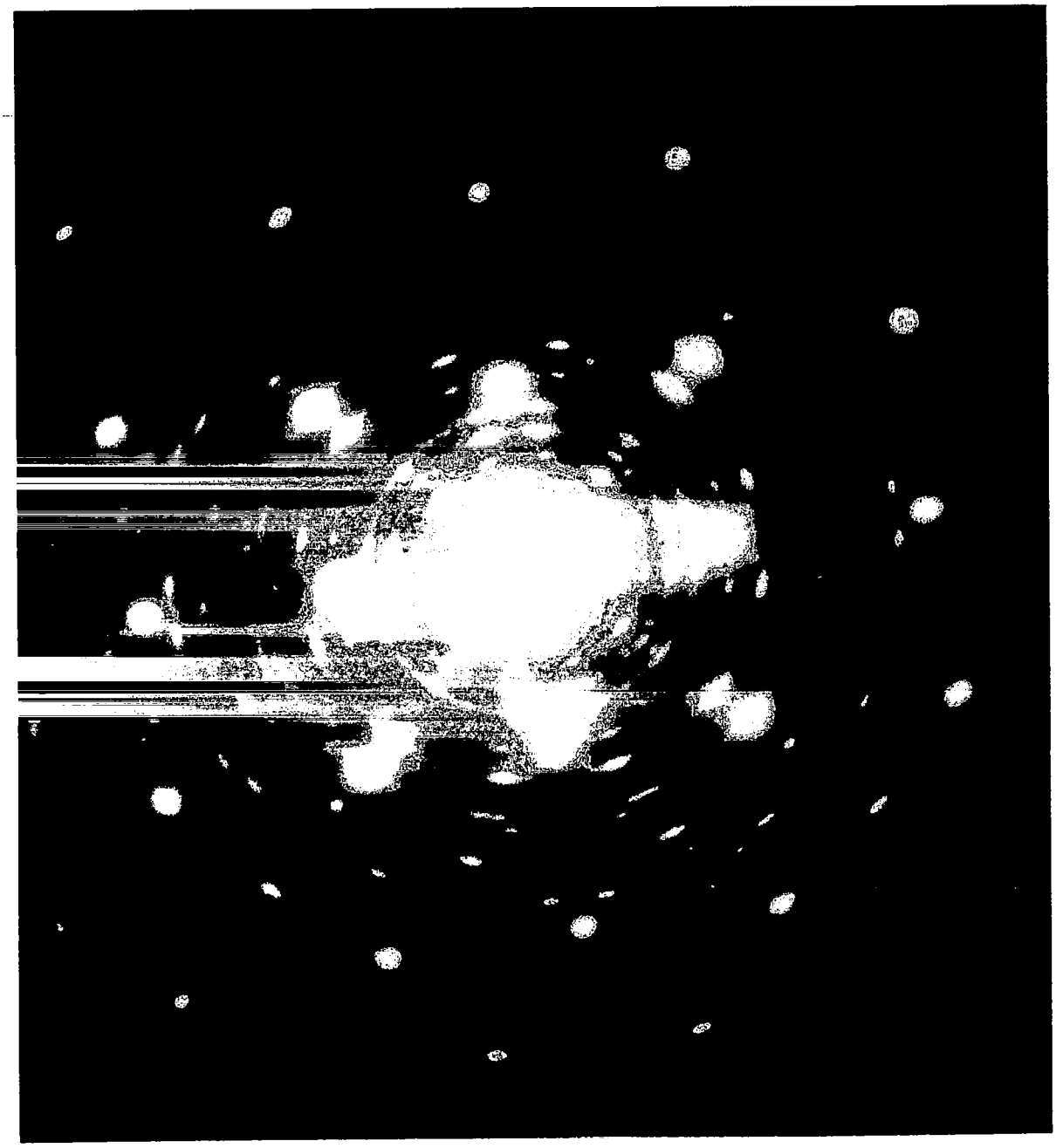

Fig. 10b

chemical corrosion process, unless:

(a) the reaction products are gaseous and cannot be determined with the technique used here, or

(b) the simulation of actual discharge conditions attempted here is insufficient; it is possible that completely different ion current densities exist at actual discharge electrodes (e.g., leading to local high surface temperatures), causing different corrosion reactions.

Gaseous electrode reaction products would be easily detected by mass spectrometer techniques but no such evidence is known to the author of this report. The possible errors introduced by insufficient simulation of actual discharge conditions, however, needed further attention. They will be examined in the next paragraph.

3.0 STUDY OF ACTUAL DISCHARGE ELECTRODE SURFACE PROCESSES (High Current Densities)

Only a small fraction of high density discharge electrode phenomena can be simulated with low current density ion bombardment studies. The majority of the electrode phenomena in which we are interested with particular respect to surface erosion problems have to be studied in actual discharge systems. Some of the important electrode processes are probably specific to certain types of "plasma gun" configurations. Only two gun types could be examined so far.

3.01 Types of Plasma Guns

The experimental facilities and laboratory support for the direct analysis of bulk cathode surface structures were provided generously by Dr. A. V. Larson's Plasma Physics Group at General Dynamics Convair. Two different

types of plasma acceleration devices were available from this group for experimentation: (1) A coaxial plasma gun developed under NASA contract NAS 3-5759. Construction details can be seen in Figure 11a. (2) A pulsed arc gun sketched in Figure 11b.* The most important operating parameters of the two guns are listed in Table 2.

	Coaxial Gun	Pulsed Arc Gun
Discharge current	200 kA	1 kA
Discharge duration	$\approx$ 2 μsec	650 μsec
Anode potential	1 kV	350 V
Cathode surface area	20 cm^2	3 cm^2
No. neutral gas particles/shot		$\approx 10^{19}$
Current sheet thickness	2 cm	
Current sheet velocity	10 cm/μsec	
Total charge density/shot	$\approx$ 0.002 Asec/cm^2	$\approx$ 0.2 Asec/cm^2
Discharge gas	NITROGEN	

TABLE 2

3.1 Search for Corrosion Products on a Copper Cathode Surface in a Nitrogen Discharge

Preliminary electrode tests with the low charge density coaxial gun had shown without doubt that severe deterioration of well polished electrode surfaces was noticed long before appreciable erosion roughening of the surfaces was found. Although the probability was high that the visible

*The interest of Dr. L. Liebing in the electrode experiments in general and his particular engagement in the pulsed arc gun tests are gratefully acknowledged.

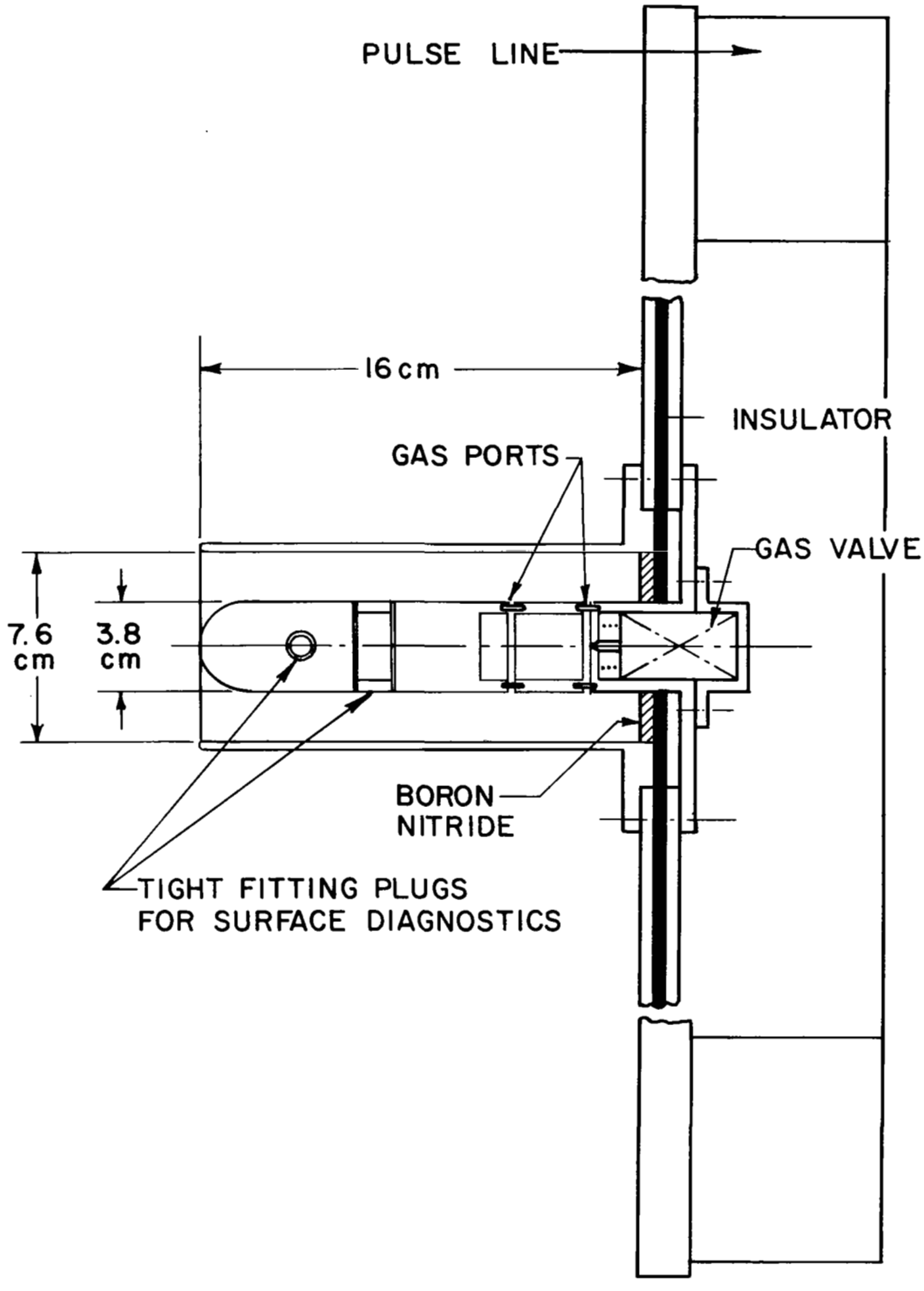
PULSE LINE
16 cm
INSULATOR
GAS PORTS
GAS VALVE
7.6 cm
3.8 cm
BORON NITRIDE
TIGHT FITTING PLUGS FOR SURFACE DIAGNOSTICS

Fig. 11a

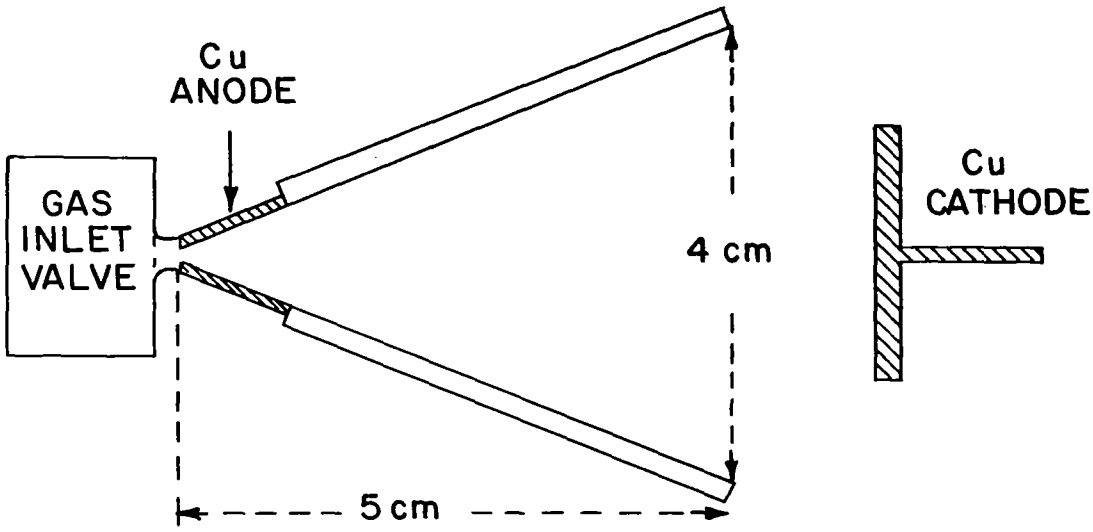

Fig. 11b

surface deterioration was due to a large extent to the bombardment cracking of residual gas hydrocarbons, the possibility of additional chemical surface attack could not be ruled out from the beginning. Therefore, the following test was performed, which was planned to supplement the low energy nitrogen ion bombardment experiments described previously (Section 2.2).

The cathode barrel of the coaxial plasma gun was modified so that small samples of the barrel surface can be studied by reflection electron diffraction methods (sample size limited by diffraction camera dimensions). For this purpose two holes of 1/4" diameter were drilled into the cathode barrel (Fig. 11a) at right angles to each other and separated by about 2 inches. Removable copper plugs were inserted and machined so that they were flush with the cathode surface. The cathode surface was polished very carefully by electrolytic means and reflection diffraction patterns were taken before the cathode was exposed to 80 shots in the coaxial gun (discharge conditions are given in Table 2). At this point the visible deterioration of the cathode surface was quite strong and the surface samples were removed to be tested again by reflection electron diffraction.

Figure 12 presents two reflexion electron diffraction patterns obtained from the cathode surface before and after exposure to the nitrogen discharge. Although the two patterns do not show the same arrangements of Debey-Scherrer rings this does not demonstrate the existence of corrosion reaction products, as an analysis of the ring patterns revealed. Corresponding to the cathode surface state before exposure to the discharge, the diffraction pattern of Figure 12a shows broad rings (due to the extremely smooth surface of the electrolytically polished cathode) in an arrangement

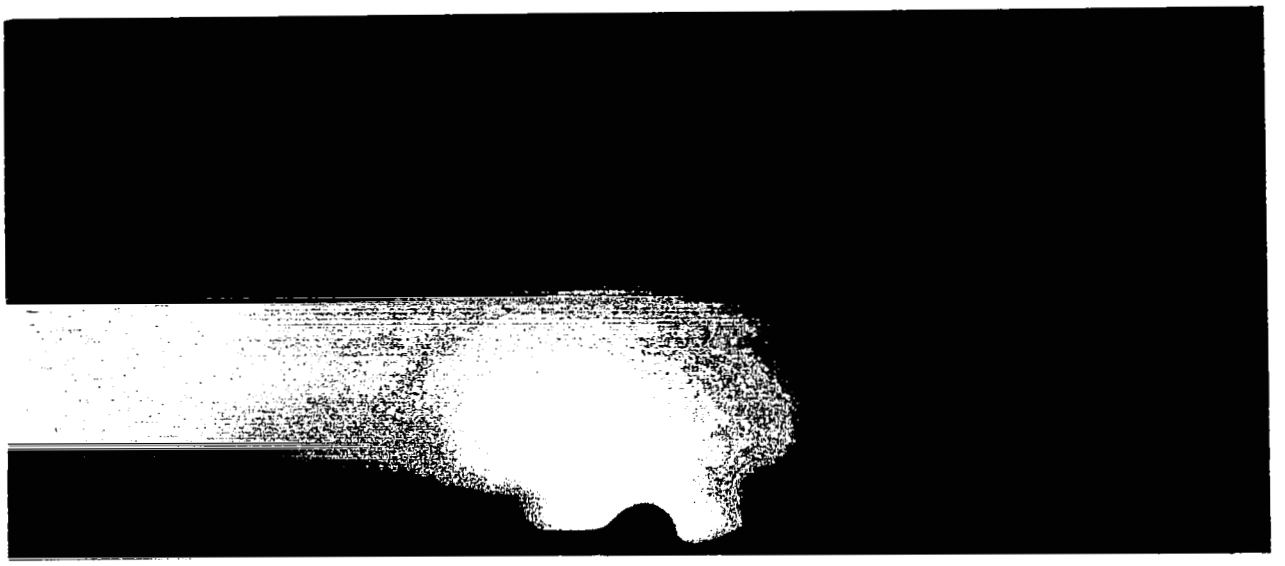

Fig. 12a

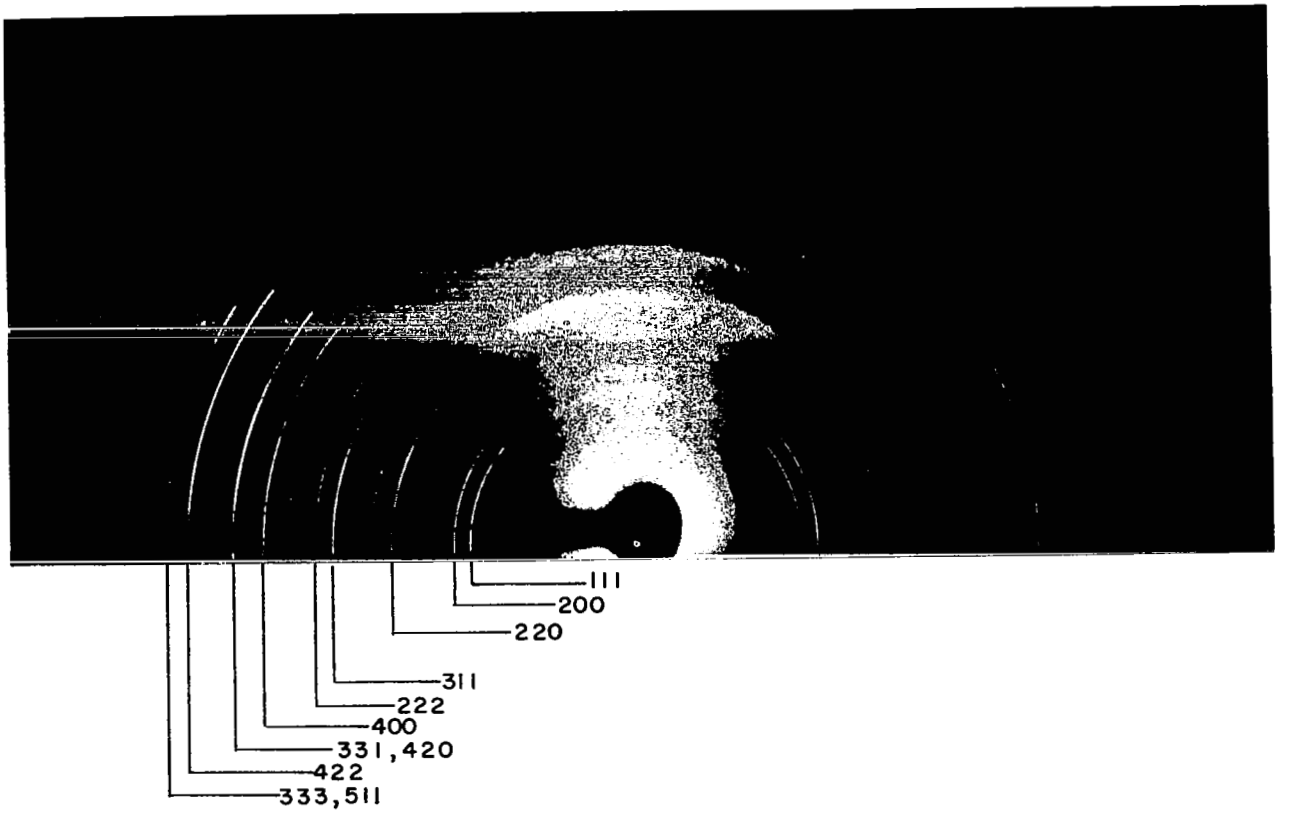

Fig. 12b

characteristic of cuprite (Cu_2O), the oxide of copper usually obtained by oxidation in air or oxygen at temperatures of up to about 200°C.[13,12]

Appearance of a sharp copper ring pattern (Figure 12b) after 80 discharge shots indicates: (a) the surface has been roughened so that the reflexion pattern approaches the character of a transmission pattern (transmission through microscopic surface asperities), (b) removal of the thin Cu_2O surface oxide layer by the discharge (probably by sputtering) or suppresion of the weak Cu_2O pattern, and (c) minimal re-oxidation during fast transfer of the cathode surface sample to the diffraction camera, probably aided by a protecting action of the carbon contamination layers.

In view of the negative results concerning chemical surface reactions in nitrogen discharges with low and high intensity nitrogen ion bombardment it has become apparent that such corrosion processes with nonvolatile reaction products do not exist under our experimental conditions, eliminating the corrosion and sputtering processes as major causes of discharge electrode destruction. Evaporation and sputtering mechanisms shall be examined in the last part of this report.

3.2 The Morphology of Eroded Electrode Surfaces

Previously we had obtained some electron diffraction information concerning changes in the micromorphology of cathode surfaces, as caused by their exposure to an increasing number of discharge shots: starting with an initially very smooth surface an increasingly rougher state of the surface developed. Electron diffraction results of this kind represent only an average state of the surface. It was hoped that more information concerning various electrode surface processes could be acquired through a detailed investigation of the changes in the topography of initially well defined electrode surfaces.

3.2.1 Surface preparation and electron microscopy replication techniques: Electrolytic polishing of initial electrode surfaces is important because a smooth surface profile is created; but it is also significant because of the removal of the debris left at the surface of any mechanically polished material. The copper cathodes

of both the coaxial and the pulsed arc gun were polished in a phosphoric acid electrolyte.

The techniques used for the preparation of electrode surface replicas for electron microscopic studies depended on the roughness of the sample surface. A one stage plastic replica method with Pt-shadowing was used for smooth surfaces. The probability of rupture of the plastic replicas was, however, too high for rougher surfaces so that here two stage carbon replicas were prepared, shadow cast again with Pt.

Usually, straight transmission electron microscopy delivers sufficient information about simple surface structures. If the morphology is more complex, however, or if it is important to avoid any ambiguity of picture interpretations sterographic transmission microscopy can be employed easily. In this case two micrographs of the same specimen area are taken with the specimen being tilted between pictures by an angle of 5° to 15°. A stero viewer helps producing an often quite remarkable stereo effect during later inspection of the two micrographs.

3.2.2 Results of replica electron microscope erosion studies: The cathode surface structure of the pulsed arc gun was studied after exposure to 3 (Figure 13a), 30 (Figure 14), and 200 (Figure 15) discharge shots, the coaxial gun cathode surface after 40,and 80 shots (Figure 16). The first and most remarkable conclusion one reaches,after inspecting these micrographs, is : for both gun types the surface damage produced during early stages of erosion is very localized and specific in character (compare, e.g., Figure 13a and Figure 16b). The localized attack would not be surprising and could have been anticipated as a special form of etching attack caused by ion bombardment if the shape of these "etch pits" were compatible with pit forms resulting from an etching mechanism. But this is definitely not the case, as the stereo observations of Figure 13a and 16b prove without doubt. Characteristic for this type of surface structure is that cathode material is rearranged so that it

protrudes over the original surface (Fig. 13b). This can only be explained by a flow of material, probably caused by localized heating that prompts the molten material to flow like lava from a crater and solidfy in layers, when reaching colder surface regions.

Not enough is known so far about the size and number statistics of these localized surface damage regions, in particular about the creation and development of the damage spots as a function of the number of discharge shots. But it seems at least plausible at this point to identify these areas with "cathode spots": localized areas of very high current densities. (Cathode spots are well known from glow discharge experiments). Comparing the surface damage caused by 3 shots of the pulsed arc gun with that caused by 80 shots of the coaxial gun, in this connection it should also be noted that the surface damage per shot in the pulsed arc gun is roughly 30 to 100 times heavier than the damage in the coaxial gun. The correlation with the total charge density values of Table 2 is obvious.

Figure 13a, 14, and 15 comprise a first attempt to study the progress of erosion damage on the pulsed arc gun cathode surface. (The simple replica techniques used up to now did not permit the repeated replication of the same specimen area in various stages of erosion). The micrographs show the development of very rough surface structures but they do not provide sufficient information for analyzing the detailed mechanism of this process. Assuming a genuine etching mechanism in addition to the thermal etching mechanism,predominating in the cathode spots, seems almost necessary in order to find an explanation for deeply etched valleys (the rims of these valleys show no sign of material flow). In Figure 14a flow- and etch-structures can be seen in the same

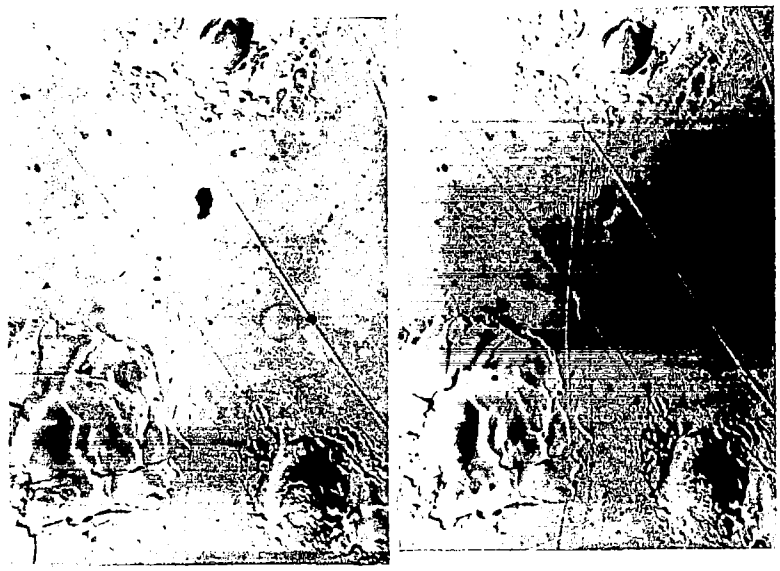

Fig. 13a

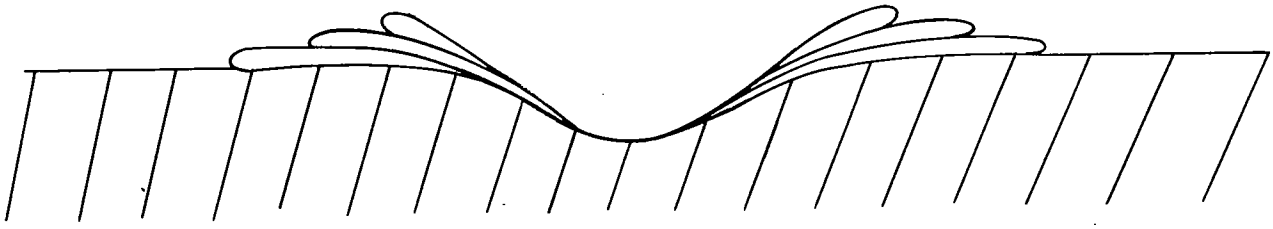

Fig. 13b

micrograph, with etch structures definitely prevailing in Figure 15. It is possible, however, that the circular regions seen in 15a and 15b represent flow structures that indicate the persistence of the cathode spot erosion mechanism.

Another interesting particular etch structure (resembling deep grooves, quite often extending from strongly eroded localized surface areas) was observed frequently. The elongated etch structures show no directionality in the case of the pulsed arc gun (upper left corner of Figure 14b) but point all in the direction of plasma flow in the case of the coaxial gun (Figure 16a). These grooves are probably the streaked topographic features observed on cathode surface light micrographs (Figure 17).

Surface features as the ones seen in Figure 16a are observed a lot more frequently on the coaxial gun surface than the flow structures presented in Figure 16b. The alignment of the direction of these shallow grooves with the axial direction of movement of the plasma current sheet is excellent. The topography, structure, and development of the grooves are still quite mysterious, although again elements of an etch- (shallow trough) and flow-mechanism (slightly protruding trough perimeter, protruding material in the center of the trough) seem to be mixed.

Concluding this paragraph, one is almost convinced that the discovery of the localized surface damage regions (flow structures) comprises an important step toward the exploration of electrode surface erosion problems. However, the replica technique that is used, in attempting to analyze the role of high current density regions and ion

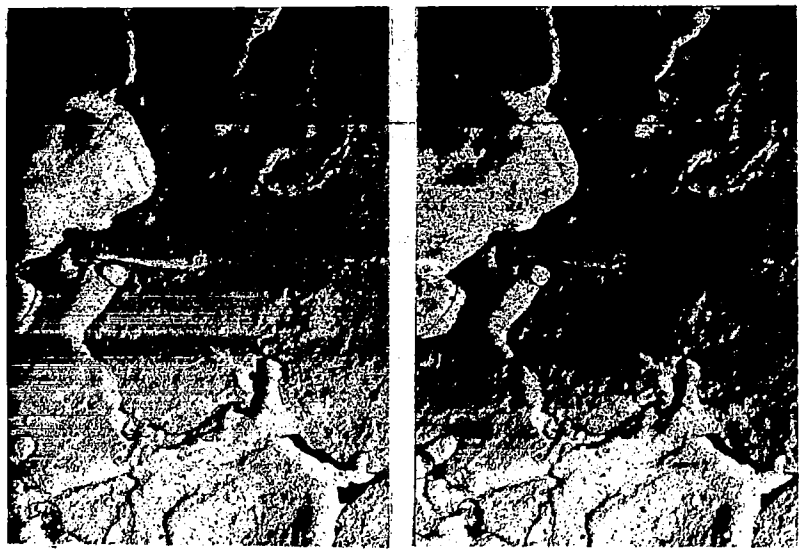

Fig. 14a

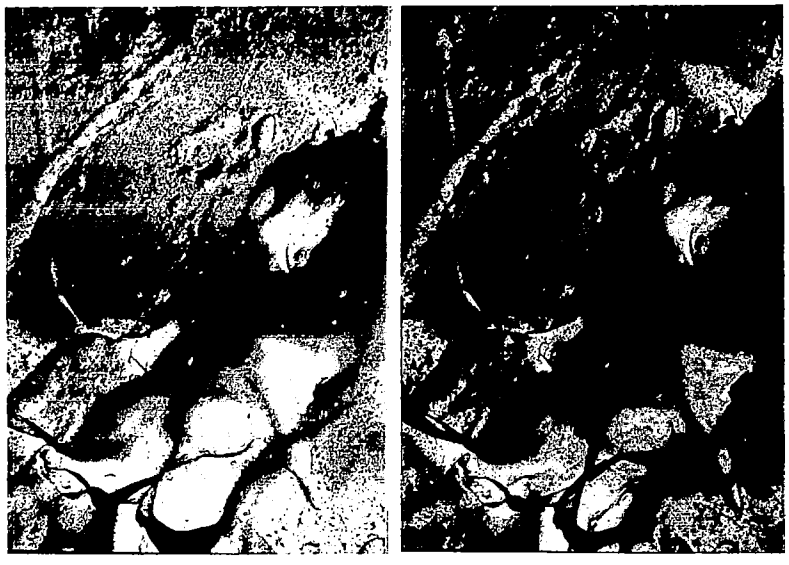

Fig. 14b

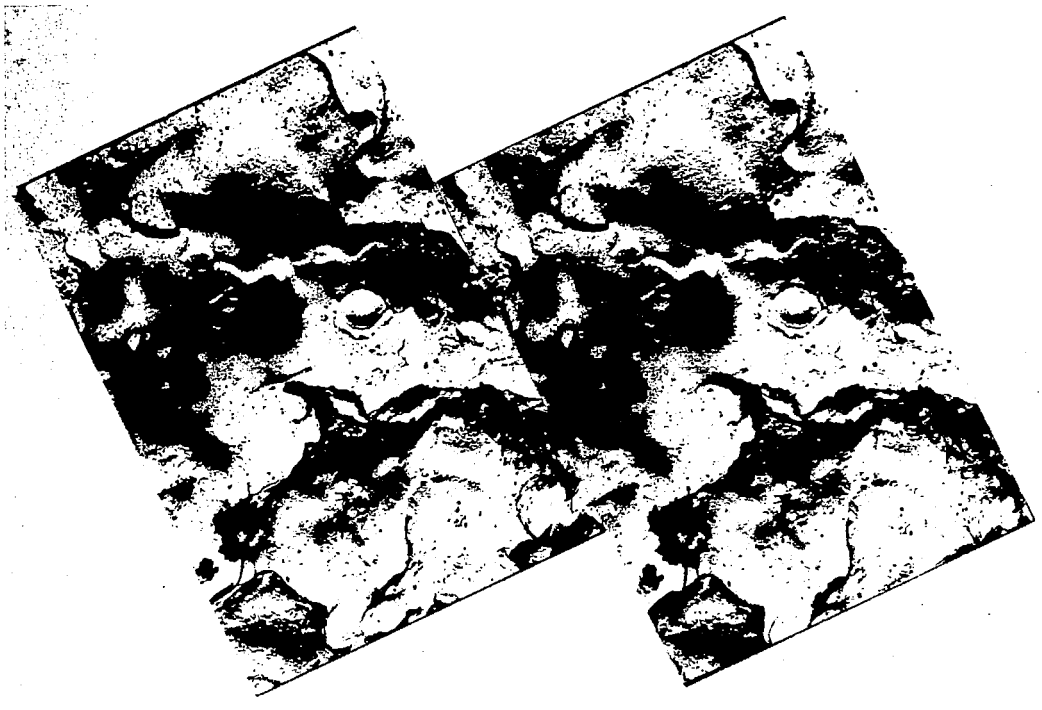

Fig. 15a

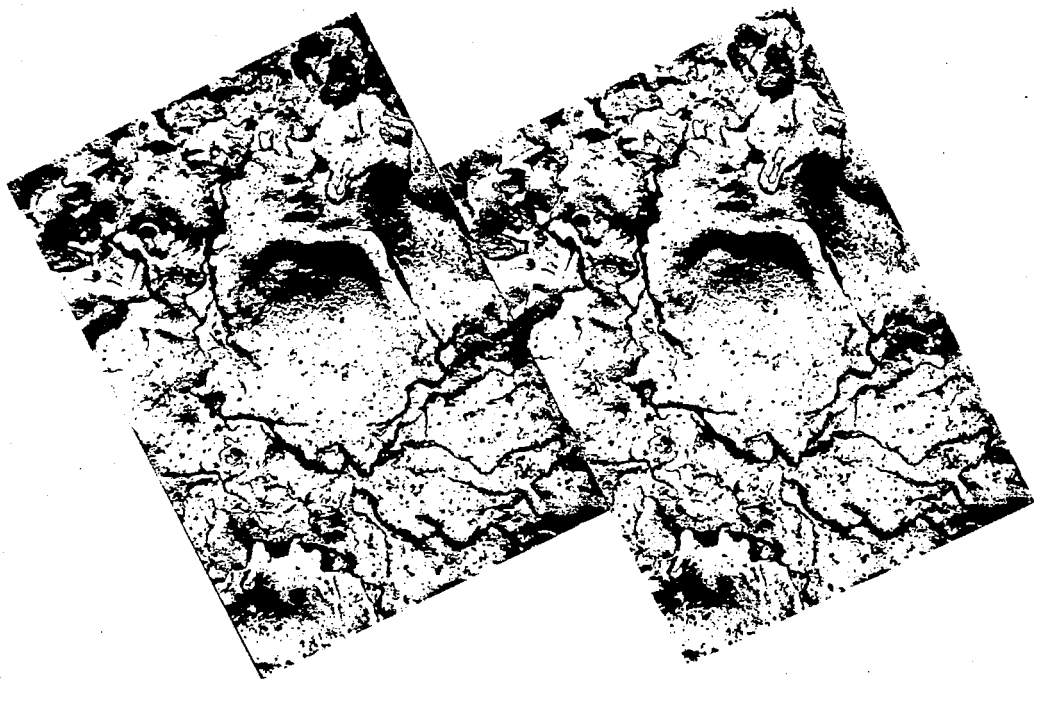

Fig. 15b

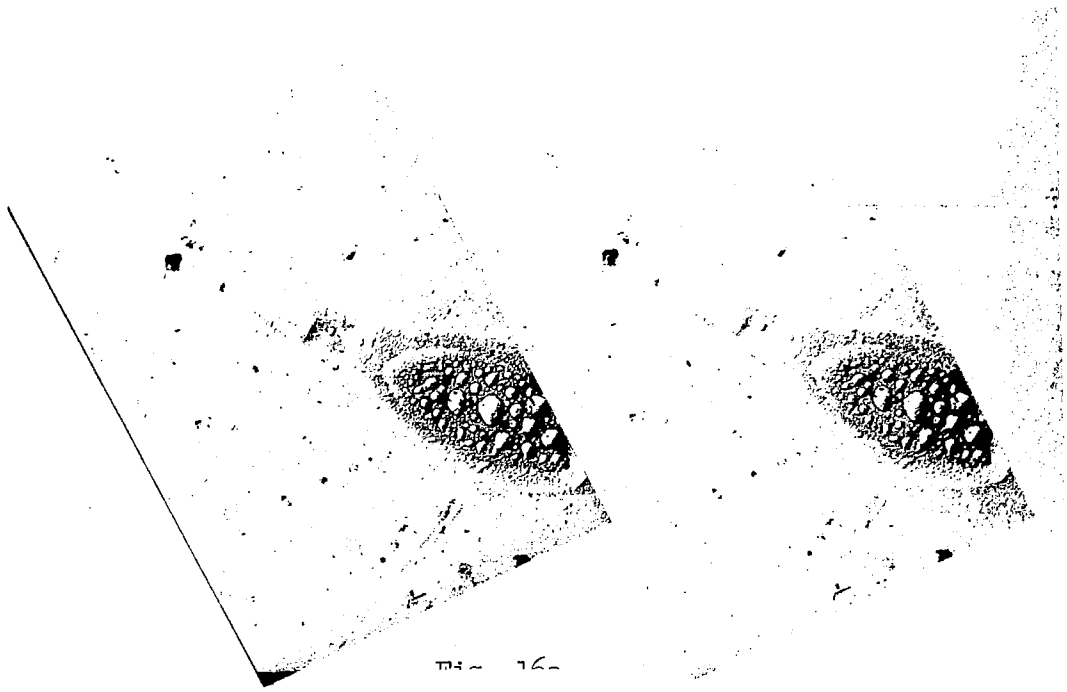

Fig. 16a

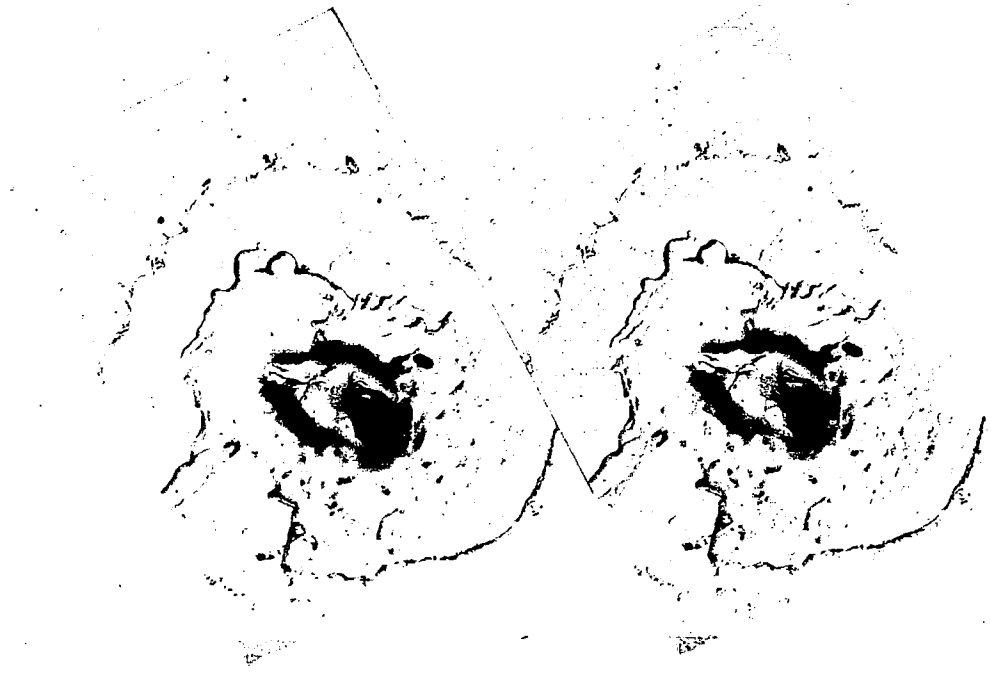

Fig. 16b

Fig. 17

bombardment sputtering processes during later stages of the erosion process, is insufficient. It seems possible that detailed pursuance of erosion processes with selected area replication methods would bring the now needed clarification: what is the relative importance of ion bombardment and thermal etching mechanisms? An answer to this question seems vital for the understanding and eventual control of the electrode erosion process.

3.3 Detection of Localized Cathode Surface Crystal Structure Changes

The concept of "cathode spots" is extremely important for further experimental and probably theoretical research concerning high current density discharge phenomena. Therefore, it was thought desirable to gather more unambiguous experimental evidence for the existence of these spots.

3.3.1 Experimental Method: From the topography of locally disturbed cathode surface areas it had been deduced that regional melting of cathode material must have occurred in the cathode spot areas ("flow structures"). An attempt was made to detect localized melting of electrode surface material by probing the crystallographic structure of a single crystal cathode surface. Selected area electron diffraction, a technique that permits recording transmission electron diffraction patterns of small specimen areas (minimum diameter of area about 1μ) selected by means of prior electron microscope inspection, was used to test the crystal structure in cathode areas where localized surface attack had occurred. Local melting and recrystallization during solidification would result in changing the cathode crystal structure from single crystal to polycrystal, the diffraction patterns from single crystal spot-to polycrystal ring-patterns.

A single crystal cathode surface that could be inspected by transmission electron microscopy means, after exposing it to a few discharge shots in the pulsed arc gun, was prepared by growing epitaxially a (111) oriented gold film on a silver-mica substrate. After the test the gold film was detached from its substrate for microscopic inspection, dissolving the underlying silver film.

Figure 18 shows the results of the selected area electron microscope tests, confirming our expectations and previous results: local melting does take place in microscopically small cathode spot areas. A thinned area surrounding a hole in the single crystal cathode film can be seen in Figure 18a; the corresponding electron diffraction pattern with well defined Debey-Scherrer rings superimposed upon the original (111) spot pattern is Figure 18b. Figures 18c and 18d illustrate the same fact with one exception: the thinned area has not yet broken through the cathode film completely. A very thin amorphous film of low sputtering yield (well known from other experiments, and probably formed at the gold-silver interface during preparation procedures) remains, spanning the hole in the gold film. A fine polycrystalline gold film (Figure 18d) with a definite island structure (similar to the structure of incomplete evaporated metal films) can be distinguished on the amorphous film (Figure 18d). It seems plausible assuming that the fine structured gold film in the hole stems from recondensing cathode material and can be viewed as direct evidence for high thermal loads in the cathode spot regions, causing evaporation of cathode material.

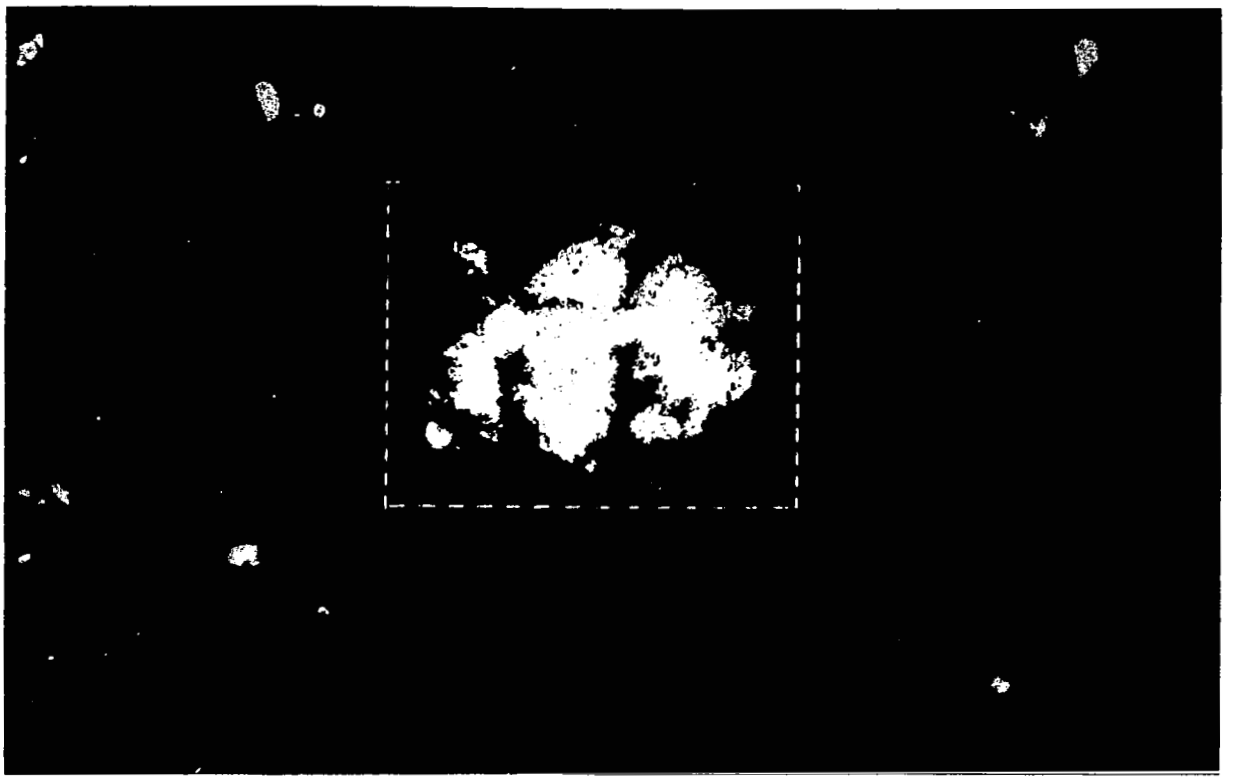

Fig. 18a

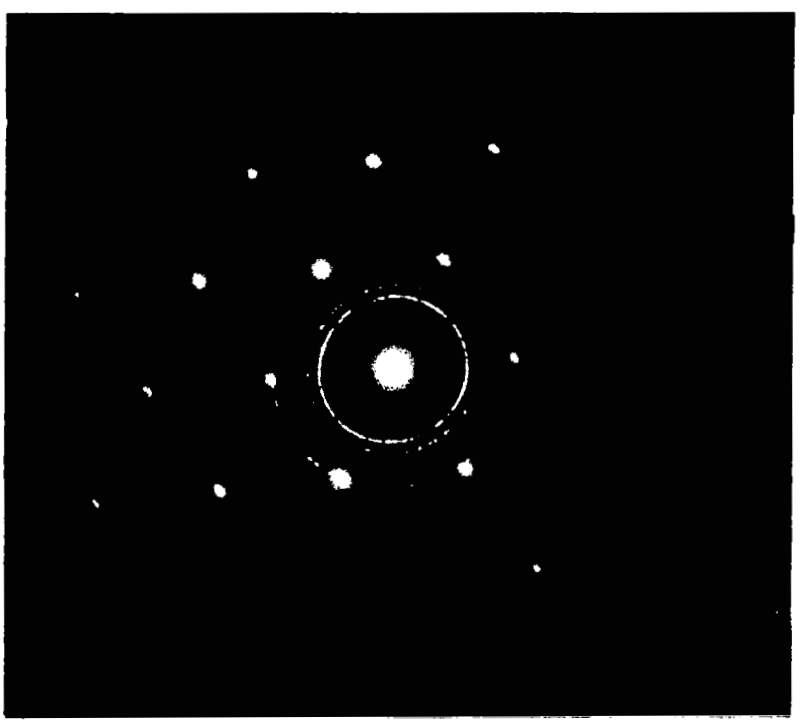

Fig. 18b

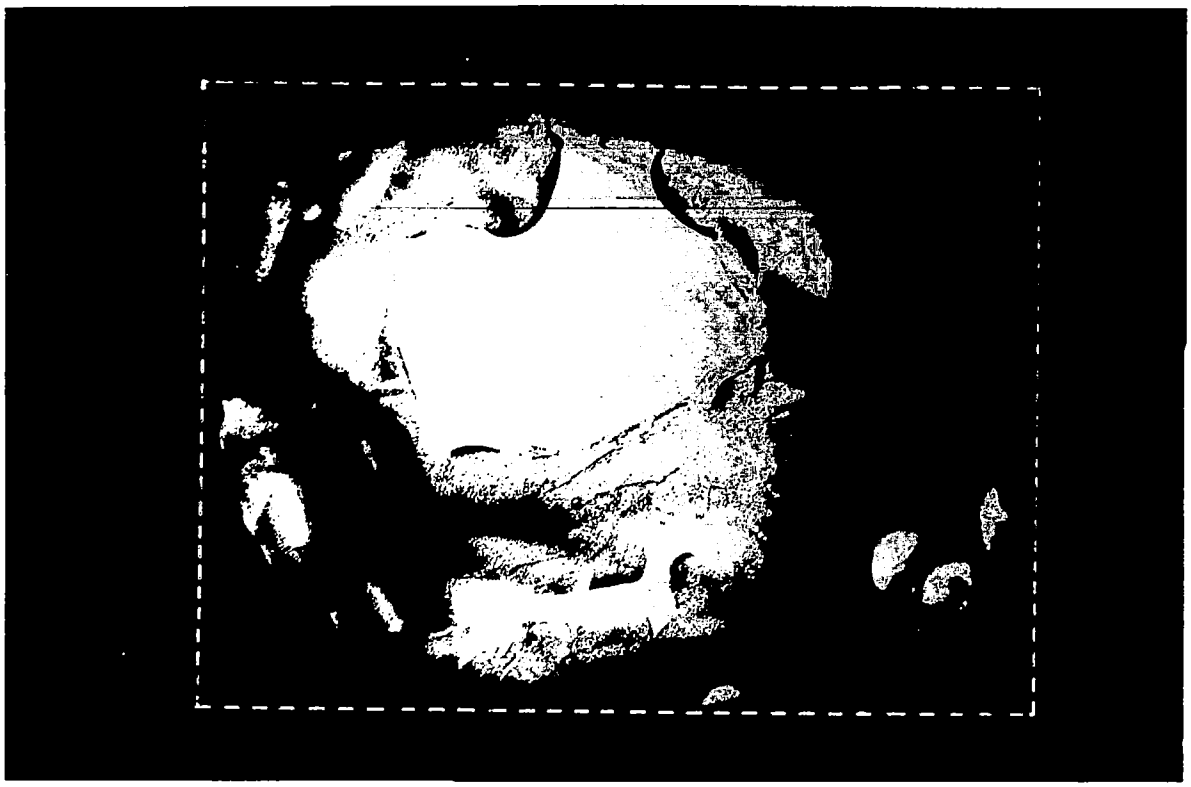

Fig. 18c

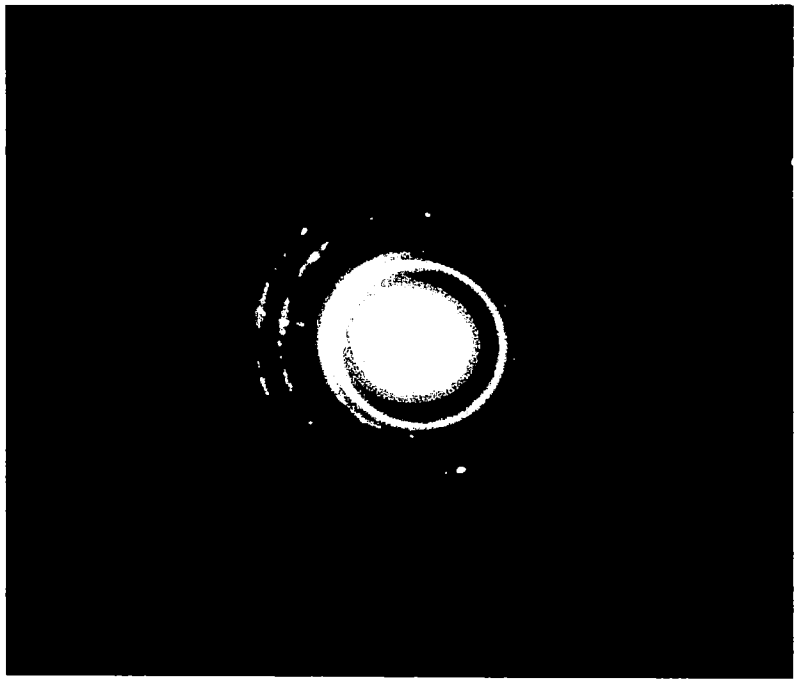

Fig. 18d

CONCLUDING REMARKS

The present investigation was undertaken primarily with the intention of gathering additional experimental information on discharge electrode erosion processes. An attempt was made to break up the complex problem of electrode destruction by recognizing, identifying, and studying a number of different surface attack mechanisms.

During this reporting period particular attention was paid to the areas of electrode surface attack by low energy ion bombardment, surface attack by chemical corrosion reactions, and surface attack by localized high current densities. While not finding any evidence for the occurrence of chemical corrosion in nitrogen discharges, the existence of cathode arc spots was found to be one of the major causes of cathode surface destruction. The cathode spots are microscopically small (5μ to 50μ in diameter) and high discharge current densities in these spots lead to localized melting and evaporation of electrode material.

At present it is not clear to what extent sputtering by discharge ions contributes to electrode erosion in high energy density discharges and what interaction, if any, exists between the arc spot and the sputtering mechanisms. Clarification of the relative importance of surface erosion by ion bombardment and thermal etching is needed now to understand better and possibly minimize discharge electrode destruction. However, the idea of minimizing sputtering attack of cathode surfaces by using properly oriented single crystal cathodes can already be discarded without awaiting future investigations in this field. The reported results on the orientation dependence of the sputtering yields of f. c. c. metals show without doubt that the influence of crystallographic orientation is too small to be of any practical importance for discharge ions of less than 500 eV energy.

APPENDIX: SYMBOLS AND UNITS

Symbols referring to the ion source schematic in Fig. 1:

U_A anode potential

U_E ion extraction potential

U_B final ion energy

I_A anode current of discharge

I_g ion current to auxiliary source electrode

I_{sp} ion current to target specimen

i_{sp} ion current density on target specimen

Length units:

$1\mu = 10^{-4}$ cm

$1\mathring{A} = 10^{-8}$ cm

Crystallographic symbols:

(111)- symbol that indicates by Miller Indices that a (111) crystal plane is parallel to the specimen surface.

REFERENCE

1. G. Ecker, Proc. Int. School Phys., "Enrico Fermi," Course XXV (1964), 97.

2. W. Finkelnburg', H. Maecker, Handb. Phys. 22 (1956), 2.

3. R. S. Nelson, Phil. Mag. 10 (1964), 343.

4. P. Bowden, D. G. Brandon, Phil Mag. 9 (1963), 935; J. Sci. Instr. 40 (1963), 213.

5. H. R. Poppa, Z. Naturf. 19a (1964), 835; Vac. Sci. Techn. 2 (1965), 42.

6. J. A. Venables, R. W. Baluffi, Phil. Mag. 11 (1965), 1021.

7. J. W. Cahn, Acta Metall. 5 (1957), 169.

8. J. D. Embury, R. B. Nicholson, Acta Metall. 13 (1965), 403.

9. G. D. Magnuson, C. E. Carlston, J. Appl. Phys. 34 (1963), 3267.

10. A. L. Southern, W. R. Willis, M. T. Robinson, J. Appl. Phys. 34 (1963), 153.

11. E. J. Zdanuk, S. P. Wolsky, J. Appl. Phys. 36 (1965), 1683.

12. Z. G. Pinsker, Electron Diffraction, Butterworth Sci. Publ. 1953, p. 262.

13. S. Miyaki, Sci. Pap. Inst. Phys. Chem. Res. Tokyo 29 (1936), 167.